JACS
JOURNAL OF THE AMERICAN CHEMICAL SOCIETY

Article

pubs.acs.org/JACS

Effects of Carbon–Metal–Carbon Linkages on the Optical, Photophysical, and Electrochemical Properties of Phosphametallacycle-Linked Coplanar Porphyrin Dimers

Yoshihiro Matano,*[,†] Kazuaki Matsumoto,[†] Hironobu Hayashi,[†] Yoshihide Nakao,[‡] Tatu Kumpulainen,[§] Vladimir Chukharev,[§] Nikolai V. Tkachenko,[§] Helge Lemmetyinen,*[,§] Soji Shimizu,[⊥] Nagao Kobayashi,*[,⊥] Daisuke Sakamaki,[†] Akihiro Ito,[†] Kazuyoshi Tanaka,[†,‡] and Hiroshi Imahori[†,‡,∥]

[†]Department of Molecular Engineering, Graduate School of Engineering, Kyoto University, Nishikyo-ku, Kyoto 615-8510, Japan

[‡]Fukui Institute for Fundamental Chemistry, Kyoto University, Sakyo-ku, Kyoto 606-8103, Japan

[§]Department of Chemistry and Bioengineering, Tampere University of Technology, P.O. Box 541, FIN-33101 Tampere, Finland

[⊥]Department of Chemistry, Graduate School of Science, Tohoku University, Sendai 980-8578, Japan

[∥]Institute for Integrated Cell-Material Sciences (iCeMS), Kyoto University, Nishikyo-ku, Kyoto 615-8510, Japan

Supporting Information

ABSTRACT: 5-(Diphenylphosphanyl)-10,15,20-triarylporphyrins (*meso*-phosphanylporphyrins) underwent complexations with palladium(II) and platinum(II) salts to afford phosphapalladacycle- and phosphaplatinacycle-fused coplanar porphyrin dimers, respectively, via regioselective peripheral β-C–H activation of the *meso*-phosphanylporphyrin ligands. The optical and electrochemical properties of these metal-linked porphyrin dimers as well as their porphyrin monomer/dimer references were investigated by means of steady-state UV–vis absorption/fluorescence spectroscopy, cyclic and differential pulse voltammetry, time-resolved spectroscopy (fluorescence and transient absorption lifetimes and spectra), and magnetic circular dichroism spectroscopy. All the observed data clearly show that the palladium(II) and platinum(II) linkers play crucial roles in the electronic communication between two porphyrin chromophores at the one-electron oxidized state and in the singlet–triplet intersystem-crossing process at the excited state. It has also been revealed that the C–Pt–C linkage makes more significant impacts on these fundamental properties than the C–Pd–C linkage. Furthermore, density functional theory calculations on the metal-linked porphyrin dimers have suggested that the antibonding dπ–pπ orbital interaction between the peripherally attached metal and adjacent pyrrolic β-carbon atoms destabilizes the highest occupied molecular orbitals of the porphyrin π-systems and accounts for the observed unique absorption properties. On the basis of these experimental and theoretical results, it can be concluded that the linear carbon–metal–carbon linkages weakly but definitely perturb the optical, photophysical, and electrochemical properties of the phosphametallacycle-linked coplanar porphyrin dimers.

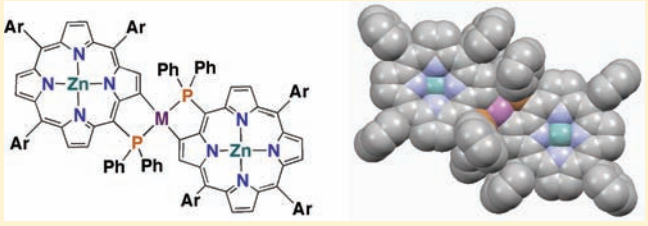

INTRODUCTION

The organization of porphyrins into well-defined multiporphyrin arrays has been the subject of extensive studies, as it has led to significant advances in not only the understanding of photoinduced events occurring in natural photosynthesis but also the development of artificial porphyrin-based materials for use in optoelectronic devices such as molecular wires and dye-sensitized solar cells. It is well-known that the efficiency of ground-state electronic coupling, exciton coupling, and electron/energy transfers among the organized multiporphyrin arrays varies dramatically depending on the distance, mutual orientation, and orbital interaction of the porphyrin subunits. In this context, the linkers (spacers) connecting two or more porphyrin rings play an important role in determining the intrinsic properties of the entire porphyrin networks.

Metal–ligand (M–L) coordinative interactions based on the precise design of the ligating groups attached at the periphery are beneficial for the construction of linear, ladder, cofacial, dendritic, and cyclic multiporphyrin architectures.[1] In particular, porphyrin dimers linked by the M–L bonds have deserved sustained interest due to their easy accessibility and structural simplicity as multiporphyrin arrays. Among the peripherally attached ligands, heterocyclic nitrogen donors such as pyridyl and imidazolyl groups have been frequently used for this purpose in combination with internal or external metals.[2] In the field of coordination chemistry, phosphorus(III) donors (tertiary phosphanes) are also used as versatile ligands toward late transition metals because of their high σ-donating and

Received: October 30, 2011
Published: December 12, 2011

dx.doi.org/10.1021/ja210205v | J. Am. Chem.Soc. 2012, 134, 1825–1839

π-accepting abilities. In the early 2000s, Sanders, Stultz, and co-workers reported an interesting protocol to use a (diphenylphosphanyl)ethynyl group as the axial ligand for metalloporphyrin assembly and predicted that incorporating the M−P coordination bonds in the supramolecular arrays would lead to complexes exhibiting attractive physicochemical properties.[3] Except for this pioneering work, however, little attention has been paid to the M−P-assisted organization of porphyrin chromophores.

In the course of our comparative studies on the M−L assisted self-assembly of *meso*-heteroatom functionalized porphyrins,[4] we were interested in the coordination chemistry of *meso*-phosphanylporphyrins that bear a *meso*-carbon−phosphorus(III) bond.[5] We envisaged that the reciprocal electronic communication between porphyrin π-systems would be achieved by the introduction of directional M−P coordination sites in close proximity to the porphyrin ring. At the initial stage, we expected that porphyrin dimers linked by two M−P bonds would be readily constructed by mixing *meso*-phosphanylporphyrins with external palladium(II) or platinum(II) salts. To our surprise, however, the M−P (M = Pd, Pt) coordination outside the porphyrin ring induced regioselective β-C−H activation of the neighboring pyrrole ring to form a fused phosphametallacycle at the periphery.[5,6] Most importantly, this cooperative M−P/M−C bond formation produced the first examples of coplanar porphyrin dimers linked by the linear carbon−metal−carbon bonds (Chart 1a).

Chart 1. Schematic Views of η^1-Metalloporphyrin Dimers:[a] (a) Present Dimers; (b) Arnold's Dimer P1;[13] (c) Osuka−Shinokubo's Dimer P2[14]

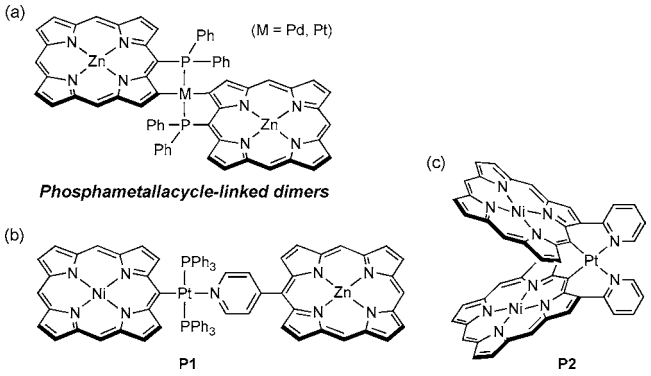

[a] *meso*-Aryl substituents are omitted for clarity.

The peripherally metalated porphyrins bearing a metal−carbon σ-bond are key intermediates in transition-metal-catalyzed cross-coupling reactions of bromo- and iodoporphyrins, which are now regarded as indispensable methods for the chemical functionalization of porphyrin rings.[7] In addition, this class of organometallic porphyrins (η^1-metalloporphyrins) offers a new concept for the construction of well-organized multiporphyrin architectures, as the peripheral metal−carbon covalent bonds are likely to define the mutual orientation of porphyrin rings through the cooperative σ and π orbital interactions that are prerequisites for efficient electronic coupling between two π-systems.[8,9] In this context, there is a need to understand the intrinsic effects of the peripheral metal−carbon bonds on the fundamental properties of the metal-linked porphyrin π-networks in both ground and excited states.

Although a variety of η^1-metallopoprhyrins have been successfully prepared and characterized by several groups,[10−12] the number of η^1-metalloporphyrin dimers is quite limited. Arnold and co-workers reported the synthesis of η^1-platinioporphyrin-containing unsymmetrical dimers such as **P1** (Chart 1b) using self-assembly reactions of *meso*-η^1-platinioporphyrin tectons with the acetylene or pyridine units of the porphyrin partners.[13] On the basis of the results obtained by absorption spectroscopy, they concluded that the peripherally attached platinum fragment acted more as a structural component than a conjugative linking group. Osuka, Shinokubo, and co-workers applied the pyridyl-assisted *meso*-C−H activation method to the synthesis of directly Pt(II)- or Pt(IV)-linked, cofacial porphyrin dimers such as **P2** (Chart 1c).[14] Quite recently, the same research group succeeded in preparing Pd-linked porphyrin nanobelts and nanobarrels (dimer, trimer, and cyclic tetramer) with remarkable curvatures via C−H activation of the corresponding β,β'-doubly 2,6-pyridylene-bridged nickelporphyrins.[15] Interestingly, these preceding examples have demonstrated that the peripherally attached metals as well as their oxidation states make significant impacts on the structural, optical, and electrochemical properties of the covalently linked porphyrin π-systems, owing to through-bond inductive effects, through-space exciton coupling, and/or steric demands. Osuka, Shinokubo, and co-workers also pointed out the importance of dπ−pπ orbital interaction between the peripheral metal and the *meso*-carbon in HOMOs of their pincer-type *meso*-platinioporphyrin monomers based on electrochemical measurements and theoretical calculations.[12] To our knowledge, however, the contribution of the dπ−pπ orbital interaction underlying the peripheral metal−carbon bonds to the electronic coupling between the metal-linked coplanar diporphyrin π-systems still remains to be elucidated.

Herein, we report full experimental and theoretical results of the optical, photophysical, and electrochemical properties of phosphametallacycle-linked coplanar porphyrin dimers bearing the palladium(II)−carbon/phosphorus or platinum(II)−carbon/phosphorus bonds (Chart 1a). Various experimental techniques including steady-state absorption and emission spectroscopy, transient pump−probe, fluorescence up-conversion, and nanosecond flash-photolysis measurements, cyclic and differential pulse voltammetry, spectroelectrochemical measurements, and magnetic circular dichroism spectroscopy were employed to disclose the intrinsic effects of carbon−metal−carbon linkages on the fundamental properties of this new class of covalently linked metalloporphyrin dimers by comparison with their porphyrin monomer/dimer references. Furthermore, the dπ−pπ orbital interaction between the peripheral metal−carbon bonds was addressed by means of density functional theory (DFT) calculations, which gave valuable insight into the experimentally observed results.

RESULTS AND DISCUSSION

1. Synthesis and Characterization. 5-(Diphenylphosphanyl)-10,15,20-triarylporphyrins (*meso*-phosphanylporphyrins) **1a−c** and 5-(diphenylthiophosphoryl)-10,15,20-triarylporphyrins (*meso*-thiophosphorylporphyrins) **2a−c** used in this study were prepared from the corresponding 5-iodo-10,15,20-triarylporphyrins according to the reported procedures including the Pd-catalyzed P−C cross coupling reaction with diphenylphosphane as a key step (for details, see Experimental Section of this paper and the Supporting Information of ref 5). These two classes of porphyrins are interconvertible by

dx.doi.org/10.1021/ja210205v | J. Am. Chem.Soc. 2012, 134, 1825−1839

Scheme 1. Sulfurization and Metal Complexations of 1a−c

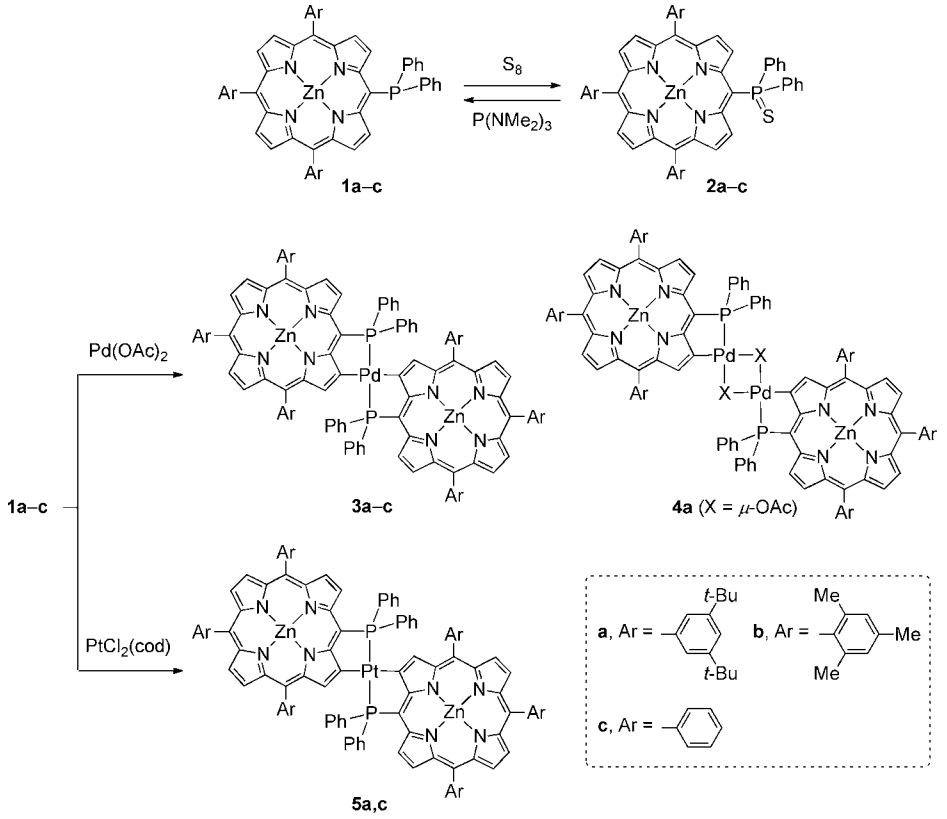

oxidative P-sulfurization (from **1** to **2**) and reductive P-desulfurization (from **2** to **1**) as shown in Scheme 1. All *meso*-phosphanylporphyrins **1a−c** are highly air-sensitive[16] and should be handled under an inert atmosphere. The ^{1}H NMR spectra of **1a−c** and **2a−c** displayed four kinds of peripheral β protons (each, 2H), reflecting C_s symmetry of these porphyrin monomers in solution. In the ^{31}P NMR spectra, a singlet peak appeared at δ −5.4 to −6.0 ppm for **1a−c** and at δ 39.0 to 40.1 ppm for **2a−c**.

The synthesis of phosphametallacycle-fused porphyrin dimers is illustrated in Scheme 1. As reported previously,[5,6] **3a,b**, **4a**, and **5a** were obtained by the reaction of *meso*-phosphanylporphyrins **1a,b** with $Pd(OAc)_2$ or $PtCl_2(cod)$ (cod =1,5-cyclooctadiene). The *meso*-phenyl-substituted phosphanylporphyrin **1c** similarly underwent complexation with a half equivalent of $Pd(OAc)_2$ and $PtCl_2(cod)$ to afford the Pd-linked porphyrin dimer **3c** and Pt-linked porphyrin dimer **5c** in 84% and 36% yields, respectively. Obviously, the *meso*-diphenylphosphanyl group in **1a−c** is capable of binding palladium(II) and platinum(II) salts in close proximity of the porphyrin ring, which eventually activates the neighboring β-C−H bond. This type of peripheral C−H activation has been utilized in the synthesis of phosphaplatinacycle- and phospharuthenacycle-fused naphthalene, anthracene, and pyrene derivatives.[17]

The phosphametallacycle-fused porphyrin dimers **3−5** are air- and moisture-stable, and their structures were characterized by conventional spectroscopic techniques. The phenyl-substituted derivatives **3c** and **5c** are less soluble than the other aryl-substituted derivatives **3a,b** and **5a**. In the mass spectra, parent ions ($[M]^+$ or $[M + H]^+$) were observed as intense peaks. The ^{31}P NMR spectra showed single peaks at δ 44.1−51.1 ppm, and the ^{1}H NMR spectra displayed seven kinds of pyrrolic β protons (each 2H) and three kinds of *meso*-aryl-derived protons. These data indicate that two porphyrin rings in **3−5** are symmetrically equivalent. The ^{31}P−^{195}Pt coupling constants of 2834 and 2810 Hz observed for the Pt-linked dimers **5a** and **5c** represent that the two phosphine ligands are coordinated in a *trans* fashion.[18] As described in our preliminary communication,[5] X-ray analysis of **3b** revealed that the palladium center in this complex adopts an essentially square planar geometry (Σ_{C-Pd-P} = 360°) with C_i symmetry, where the two porphyrin rings are almost on the same plane with a Zn−Zn (center-to-center) distance of 12.1 Å. Although the quality of X-ray data for **5a** is not at the publishable level, the structural features of the Pt-linked porphyrin dimer **5a** were found to be close to those of **3b**.

2. Optical Properties. Compounds **3** and **5** are the first examples of coplanar porphyrin dimers linked by carbon−metal−carbon (C−M−C) bonds. Hence, it is of utmost importance to reveal the intrinsic effects of the peripheral C−M−C linkages on the optical properties of the covalently linked diporphyrin π-systems. Table 1 summarizes the steady-state UV−vis absorption data of **2a−c**, **3a−c**, **4a**, and **5a,c** and Figure 1 depicts the normalized absorption spectra of the 3,5-di(*tert*-butyl)phenyl-substituted derivatives **2a**, **3a**, **4a**, and **5a** in toluene. In the spectrum of *meso*-thiophosphorylporphyrin **2a**, an intense Soret band and relatively weak Q bands were observed at λ_{max} 434 nm and λ_{max} 560/600 nm, respectively. The bis-μ-acetato-bridged porphyrin dimer **4a** showed a slightly broadened Soret band at 438 nm probably due to weak exciton coupling between the two chromophores; however, the whole spectral features of **4a** largely resemble those of the porphyrin monomer **2a**. By contrast, the Pd-linked dimer **3a** and Pt-linked dimer **5a** exhibited unusual spectral features.

dx.doi.org/10.1021/ja210205v | J. Am. Chem.Soc. 2012, 134, 1825−1839

Table 1. ^{31}P Chemical Shifts and UV−vis Absorption Data for 2−5

compound	δ_P/ppm[a]	λ_{max}/nm[b] (log ε)
2a	40.1	434 (5.45), 560 (4.12), 600 (3.94)
2b	39.0	433 (5.56), 559 (4.21), 598 (4.03)
2c	39.8	433 (5.53), 559 (4.20), 598 (4.03)
3a	51.1	426 (5.63), 554 (4.77), 583 (4.18), 601 (4.49)
3b	48.6	422 (5.37), 556 (4.53), 583 (4.08), 600 (4.28)
3c	48.3	423 (5.22), 555 (4.37), 583 (3.84), 600 (4.08)
4a	50.5	438 (5.74), 552 (4.58), 582 (4.15), 601 (4.35)
5a	46.7[c]	422 (5.46), 562 (4.59), 592 (4.20), 610 (4.43)
5c	44.1[d]	421 (5.36), 562 (4.48), 592 (4.16), 609 (4.31)

[a]Measured in $CDCl_3$ or CD_2Cl_2. [b]Measured in toluene. [c]J_{PPt} = 2834 Hz. [d]J_{PPt} = 2810 Hz.

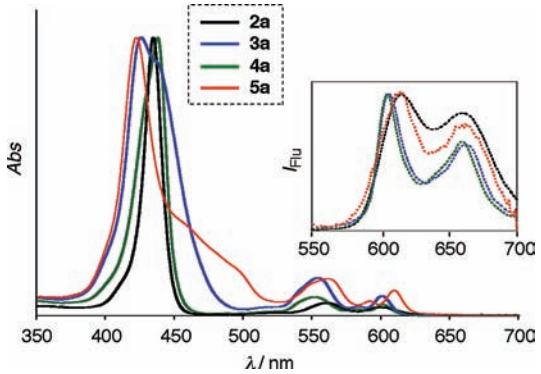

Figure 1. Normalized steady-state UV−vis absorption (solid line) and fluorescence (inset; dotted line) spectra of **2a** (black), **3a** (blue), **4a** (green), and **5a** (red) in toluene.

As shown in Figure 1, **3a** showed split Soret bands at 426 and 438 (sh) nm, whereas **5a** showed a relatively sharp Soret band at 422 nm together with unusually broad absorptions at around 450−500 nm. The spectral shapes of the other *meso*-aryl-substituted derivatives **2b**,**c**, **3b**,**c**, and **5c** (Figures S1 and S2 in the Supporting Information) are almost identical to those of **2a**, **3a**, and **5a**, respectively. It is likely that the through-bond interaction at the C−M−C linkages (M = Pd, Pt) produces these unique absorption properties. The above-mentioned spectral features will be discussed in more detail in the following sections.

The normalized steady-state fluorescence spectra of **2a**, **3a**, **4a**, and **5a** in toluene are summarized in an inset of Figure 1. Upon excitation of the Soret bands of **2a**, **3a**, **4a**, and **5a**, two emission bands that are characteristic of fluorescence from the first excited singlet (S_1) state of zinc porphyrin chromophores were observed in the range of 550−800 nm with emission maxima (λ_{em}) of 605−616 and 658−663 nm. It should be noted that the spectral shape and transition energies of the fluorescence observed for **3a** are almost identical to those observed for **4a**. This implies that both **3a** and **4a** essentially exhibit the character of the β−η^1-palladioporphyrin chromophore in their excited states. Fluorescence quantum yields (Φ_f) of **2a**, **3a**, **4a**, and **5a** were determined by using 5,10,15,20-tetraphenylporphyrin (TPP) as a reference (Φ_f = 0.11),[19] where the excitation wavelength was 425 nm for all cases. The phosphapalladacycle-fused porphyrin dimers **3a** (Φ_f = 0.0061) and **4a** (Φ_f = 0.0035) are weakly fluorescent compared to *meso*-thiophosphorylporphyrin **2a** (Φ_f = 0.030). The emitting ability of the Pt-linked dimer **5a** (Φ_f = 0.0032) is half as large as that of the Pd-linked dimer **3a**. It is apparent that the peripherally attached palladium and platinum atoms enhance the relative rate of the nonradiation pathway from the S_1 state (*vide infra*).

3. Photophysical Properties. To obtain a deep insight into the photodynamics of the present phosphametallacycle-linked coplanar porphyrin dimers, we first measured the fluorescence lifetimes of **2a**,**b**, **3a**,**b**, and **5a** in toluene by using a time-correlated single-photon-counting (TCSPC) technique (λ_{ex} = 405 nm) with a time-resolution of 100 ps. In each measurement, emission data were collected at both of the fluorescence maxima. For instance, the fluorescence decay curves of **2a** and **2b** were fitted as a single exponential with lifetimes of 0.78 and 0.62 ns, respectively. On the other hand, the time-resolution of the TCSPC instrument was too low to resolve the lifetimes for the metal-linked porphyrin dimers **3a**,**b** and **5a**. Therefore, we measured their fluorescence lifetimes by using a femtosecond up-conversion technique to determine them more accurately. The fluorescence decay curves were analyzed by two-exponential decay fittings (Figure S3 in the Supporting Information). The contribution of the minor component was found to be negligible for **2a** and **3b**. The curve fittings of **2b**, **3a**, and **5a** yield the minor components (9−15%) with the longer lifetimes, which might derive from trace amounts of fluorescent zinc porphyrin impurities produced during the experimental conditions. Table 2 summarizes the fluorescence lifetimes of the major components (τ_S) obtained by the up-conversion method; τ_S values of **2a**, **2b**,

Table 2. Lifetimes (τ), Quantum Yields (Φ), and Calculated Rate Constants (k) of 2a,b, 3a,b, and 5a

	2a	**2b**	**3a**	**3b**	**5a**
τ_S/ps[a]	710	520	57	62	4
τ_{ic}/ps[b]	0.45	0.60	0.26	0.60	3.8
τ_{isc}/ps[b]	410	430	56	26	4 and 137
τ_T/μs[c]	1.15 (0.70)	n.d.	1.36 (0.59)	n.d.	1.60 (0.48)
Φ_f[d]	0.030	0.027	0.0061	0.0038	0.0032
Φ_{isc}	0.97	0.97	0.99	∼1.0	∼1.0
k_{ic}/s^{-1}	2.2×10^{12}	1.7×10^{12}	3.8×10^{12}	1.7×10^{12}	n.d.
k_f/s^{-1}	4.2×10^{7}	5.2×10^{7}	1.1×10^{8}	6.1×10^{7}	8.0×10^{8}
k_{isc}/s^{-1}	1.4×10^{9}	1.9×10^{9}	1.8×10^{10}	1.6×10^{10}	2.5×10^{11}[e]
k_T/s^{-1}	8.7×10^{5}	n.d.	7.4×10^{5}	n.d.	6.3×10^{5}

[a]Determined by up-conversion technique (λ_{ex} = 410 nm). [b]Determined by femtosecond pump−probe technique. [c]Determined by nanosecond flash photolysis under N_2 atmosphere. The values in parentheses are those determined in air. [d]λ_{ex} 425 nm; referenced to 5,10,15,20-tetraphenylporphyrin (Φ_f = 0.11[20]). Abbreviations: S, singlet; T, triplet; ic, internal conversion; f, fluorescence; isc, intersystem crossing; n.d., not determined. [e]$k_{isc} + k'_{isc} \sim k_{isc}$ ($k_{isc} \gg k'_{isc}$).

dx.doi.org/10.1021/ja210205v | J. Am. Chem.Soc. 2012, 134, 1825−1839

3a, **3b**, and **5a** are 0.71, 0.52, 0.057, 0.062, and 0.004 ns, respectively. It is apparent that the peripherally attached palladium(II) and platinum(II) atoms shorten the lifetimes considerably. A very small difference in τ_S values between **3a** (0.057 ns) and **3b** (0.062 ns) implies that the *meso*-aryl substituents do not influence the photodynamics of the Pd-linked zinc porphyrin dimers.

Next, time-resolved transient pump−probe absorption measurements in the subpicosecond time domain were carried out for **2a**,**b**, **3a**,**b**, and **5a** with excitation at 410 nm, corresponding to the S_0−S_2 transition of the zinc porphyrin chromophores. An exponential decay model with a three-component approximation reasonably analyzed the raw data.[20] For all the compounds examined, a long-lived transient state was formed in time less than 1 ns. The representative results obtained for **3b** are summarized in Figure 2: (a) transient

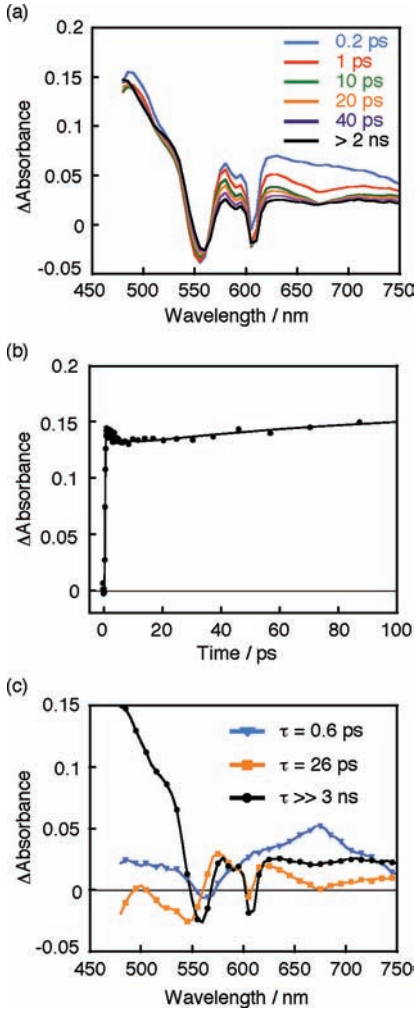

Figure 2. Representative results on the time-resolved pump−probe measurements obtained for **3b**: (a) Subpicosecond transient absorption spectra in toluene excited at 410 nm. (b) Time trace of transient signals monitored at 480 nm. (c) Time-resolved component spectra and their lifetimes (τ) determined by the 3-exponential decay model.

absorption spectra, (b) decay/formation curves, and (c) component spectra obtained by fitting with three exponentials. The component spectra and their calculated lifetimes for **2a**,**b**, **3a**, and **5a** are summarized in Figure S4 in the Supporting Information. Qualitative analyses of the spectroscopic data are based on previous studies on the photodynamics of typical zinc porphyrin chromophores.[21]

The first decaying component of *meso*-thiophosphorylporphyrins **2a**,**b** (τ = 0.45−0.6 ps) and Pd-linked dimers **3a**,**b** (τ = 0.26−0.6 ps) can be regarded as the second excited singlet (S_2) state. The second decaying component of **2a**,**b** and **3a**,**b** is most likely the S_1 state, as their lifetimes (τ = 410−430 ps for **2a**,**b**; τ = 26−56 ps for **3a**,**b**) correspond to those determined by the up-conversion measurements (τ_S = 0.52−0.71 ns for **2a**,**b**; τ_S = 57−62 ps for **3a**,**b**). The third, long-living transient species (τ > 3 ns) with a broad absorption at around 500 nm is most probably the first excited triplet (T_1) state (*vide infra*). The Pt-linked dimer **5a** showed a different behavior. The long-living transient species seems to be formed by two different states with different rates, one with a formation time of 4 ps and the other with a formation time of 137 ps. The transient species with the shorter lifetime corresponds to the major component observed by the up-conversion method (τ_S = 4 ps) and can be assigned as the S_1 state of the zinc porphyrin chromophore, while the nature of the transient species with the longer lifetime is unclear at present. Again, the final long-living transient species is reasonably assigned as the T_1 state. The formation and decay of the T_1 state were confirmed by independent nanosecond flash-photolysis experiments of **2a**, **3a**, and **5a** in the presence and absence of oxygen (Figure S5 in the Supporting Information). As summarized in Table 2, the lifetimes of the T_1 states (τ_T) were largely decreased in the presence of oxygen. In all cases, the transient spectra obtained by the flash-photolysis technique match perfectly with those of the long-living components obtained by the pump−probe technique.

With all these data in hand, we quantified the effects of the peripherally attached metals on the photophysical properties of the phosphametallacycle-linked porphyrin chromophores (Figure 3). For all the porphyrin derivatives examined,

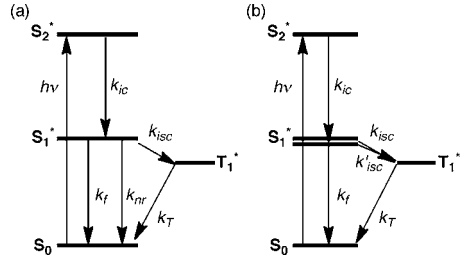

Figure 3. Photophysical processes of zinc porphyrin chromophores in (a) **2**, **3**, and (b) **5**.

a decrease of the S_1 state is concomitant with the formation of the T_1 state. As the lifetimes of the S_1 states (τ_S) analyzed by the pump−probe technique are close to those determined by the up-conversion method, it is reasonable to assume that $k_f + k_{isc} \gg k_{nr}$, and therefore $k_f + k_{isc} \approx k_0$. On the basis of the ordinary kinetics with this assumption ($\Phi_f = k_f/k_0$; $k_0 \approx k_f + k_{isc}$; $\tau_{ic} = 1/k_{ic}$; $\tau_{isc} = 1/k_{isc}$; $\tau_S = 1/k_0$; $\tau_T = 1/k_T$), the rate constants, k_{isc}, k_f, k_{isc}, and k_T, of **2a**,**b**, **3a**,**b**, and **5a** were calculated and summarized in Table 2. The rate constants of the internal conversion from the S_2 to S_1 state for **2a**,**b** and **3a**,**b** (k_{ic} = (1.7−3.8) × 10^{12} s^{-1}) are comparable to the reported value (k_{ic} = 3 × 10^{12} s^{-1}) for [5,10,15,20-tetraphenylporphyrinato]zinc.[21d] In all cases, the rate constants of the intersystem crossing (k_{isc}) are 2−3 orders of magnitude larger than those of the fluorescence

dx.doi.org/10.1021/ja210205v | J. Am. Chem.Soc. 2012, 134, 1825−1839

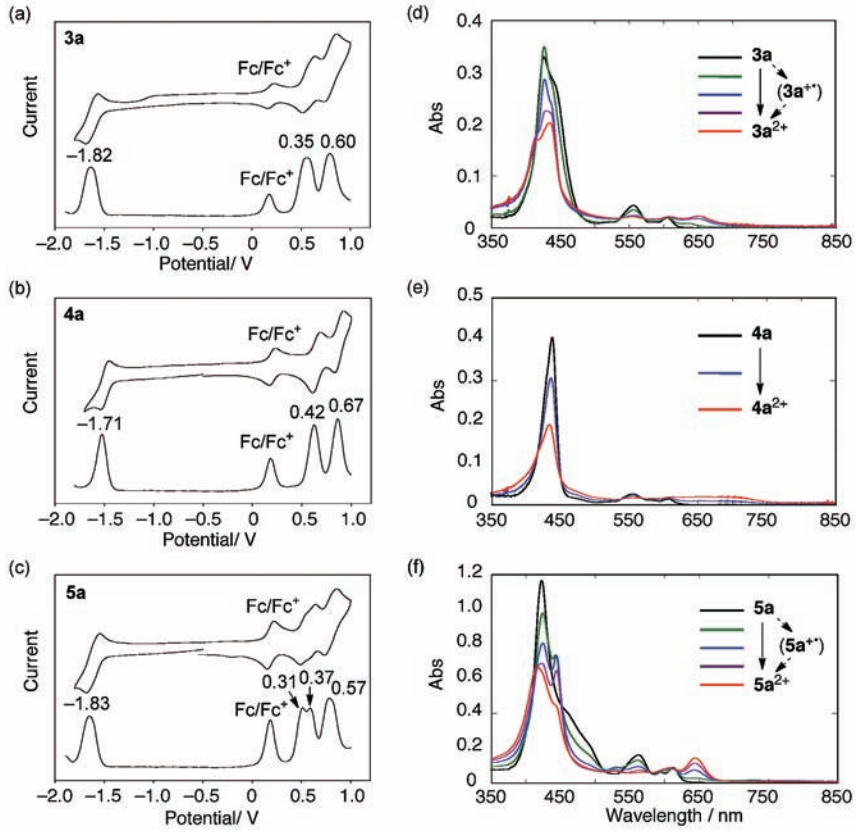

Figure 4. (a)−(c) Cyclic voltammograms (upper) and differential pulse voltammograms (lower) in the range of −2.0 to 1.0 V for (a) **3a**, (b) **4a**, and (c) **5a**. Measured in CH_2Cl_2 with 0.1 M Bu_4NPF_6 as a supporting electrolyte; Ag/Ag^+ [$AgNO_3$ (MeCN)] as a reference electrode; Scan rate 20 mV s^{-1}. Redox potentials (in V) relative to that of Fc/Fc^+ are shown above DPV voltammograms. (d)−(f) Spectroscopic changes observed in the electrochemical oxidation processes from (d) **3a**, (e) **4a**, and (f) **5a** to their dication species in CH_2Cl_2 containing 0.1 M of Bu_4NPF_6.

decay (k_f), and both k_{isc} and Φ_{isc} values gradually increase in the order: **2a,b** < **3a,b** < **5a**. It is evident that the peripherally attached palladium and platinum metals exhibit heavy-atom effects on the singlet−triplet mixing. The k_{isc} value of **5a** (2.5×10^{11} s^{-1}) estimated from the faster decaying component (τ_{isc} = 4 ps) is about 15 times larger than that of **3a** (1.8×10^{10} s^{-1}), indicating that the β-platinio group enhances the spin−orbit coupling more efficiently than the β-palladio group. The metastable excited state (τ_{isc} = 137 ps, k'_{isc} = 7.3×10^9 s^{-1}) observed for **5a** might involve the Pt−C bonding interaction. The T_1 states of the metal-linked dimers **3a** and **5a** were found to decay with almost the same rate constants (k_T = (6.3−7.4) × 10^5 s^{-1}). To our knowledge, this is the first comprehensive study to reveal the photodynamics of the peripherally metalated porphyrin derivatives. The attachment of the phosphapalladacycles and phosphaplatinacycles has proven to dramatically accelerate the formation of the T_1 state of the porphyrin chromophores.

4. Electrochemical Properties. To investigate electronic effects of the C−M−C linkages on the redox properties of the phosphametallacycle-linked coplanar porphyrin dimers, redox potentials of **3a,b**, **4a**, and **5a** were measured in CH_2Cl_2 by means of cyclic voltammetry (CV) and differential pulse voltammetry (DPV) in the range of −2.0 to +1.0 V (vs Ag/Ag^+) with Bu_4NPF_6 as a supporting electrolyte. The voltammograms of the electrochemical oxidation and reduction processes observed for **3a**, **4a**, and **5a** are summarized in Figure 4a−c. The bis-μ-acetato-bridged zinc porphyrin dimer **4a** (Figure 4b) showed two reversible oxidation processes at +0.42 V (2e) and +0.67 V (2e) and a reversible reduction process at −1.71 V (2e). The bis(μ-acetato) bridges in **4a** are unlikely to promote the electronic communication between the two porphyrin π-systems in the 1e-oxidized states. The coplanar, Pd-linked porphyrin dimer **3a** (Figure 4a) showed two oxidation processes at +0.35 V (2e) and +0.60 V (2e) and the reduction process at −1.82 V (2e), all of which were shifted cathodically by 0.07−0.11 V relative to those of **4a**. It is worth noting that a full width at half-maximum (fwhm) of the first oxidation peak in DPV of **3a** (ca. 0.18 V; scan rate = 20 mV s^{-1}) is somewhat larger than that of **4a** (ca. 0.12 V). This is presumably due to a small splitting of the first oxidation process of **3a**. Indeed, the mesityl-substituted Pd-linked dimer **3b** showed two overlapping peaks for the first oxidation process at +0.34 V (1e) and +0.38 V (1e), which was followed by the second oxidation process at +0.66 V (2e). The splitting of the first oxidation process was more distinct for the Pt-linked dimer **5a** (Figure 4c), wherein reversible voltammograms were observed at +0.31 (1e), +0.37 (1e), and +0.57 V (2e) for the oxidation processes and at −1.83 V (2e) for the reduction process. The first oxidation potential (E_{ox}) of the Pt-linked dimer **5a** shifted cathodically by 0.04 V relative to that of the Pd-linked dimer **3a**, whereas the first reduction potential (E_{red}) of **5a** is very close to that of **3a**. Accordingly, the electrochemical HOMO−LUMO gap (E_{ox}–E_{red}) of **5a** (2.14 V) is slightly smaller than that of **3a** (2.17 V), which is in good agreement with the difference in the optical HOMO−LUMO gaps between **5a** (2.03 eV) and **3a** (2.06 eV) as determined by their absorption/emission spectra in toluene. These observations primarily

dx.doi.org/10.1021/ja210205v | J. Am. Chem.Soc. 2012, 134, 1825−1839

indicate the presence of electronic coupling of the two porphyrin π-systems through the C−M−C linkages in **3a**,**b** and **5a**. It is also evident that **5a** is slightly easier to electrochemically oxidize than **3a**.

In the CV and DPV measurements of covalently linked porphyrin dimers, the 1e/1e/2e (in some cases, 1e/1e/1e/1e) electrochemical oxidation processes have been frequently observed, and the intriguing roles of arene (phenylene, naphthalene, etc.), vinylene, acetylene, and butadiyne linkers have been discussed in detail.[22] It is well-known that the degree of electronic coupling between two porphyrin π-systems is reflected in the potential difference between the first and second 1e-oxidation steps (ΔE_{ox}), corresponding to the successive formation of the π-radical monocation and dication; the stronger the electronic coupling is, the larger ΔE_{ox} is. In this context, the electronic coupling through the C−Pt−C bond in **5a** is considered to be larger than that through the C−Pd−C bond in **3a**. To our knowledge, the literature contains only a few studies on the redox properties of metal-linked coplanar porphyrin dimers (Chart 2). Yeh and co-workers reported that

Chart 2. Yeh's Pt-Linked Dimer P3[23] and Callot's Palladacycle-Linked Dimers P4[24]

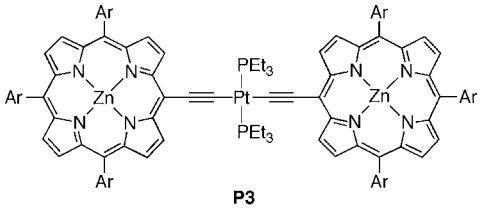

P3

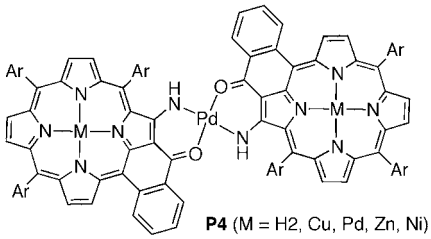

P4 (M = H2, Cu, Pd, Zn, Ni)

(Ar = 3,5-(*t*-Bu)$_2$C$_6$H$_3$)

the platinum(II) diacetylide-bridged zinc porphyrin dimer **P3** showed oxidation potentials at +0.50 (1e), +0.56 (1e), and +1.01 (2e) V in CH_2Cl_2.[23] Callot and co-workers reported that the doubly palladacycle-fused coplanar porphyrin dimers **P4** displayed split voltammograms with ΔE_{ox} of 0.13−0.17 V, although the redox properties of the zinc porphyrin analogue were not included.[24] The potential difference of the present Pt-linked zinc porphyrin dimer **5a** (ΔE_{ox} = 0.06 V) is comparable to that of **P3** (ΔE_{ox} = 0.06 V) but appreciably smaller than the values reported for acetylene- and butadiyne-linked zinc porphyrin dimers (ΔE_{ox} = 0.09−0.13 V).[25,26] In addition, the electrochemical HOMO−LUMO gaps (differences between the first oxidation and reduction potentials) of **3a** (ΔE_{HL} = 2.14 V) and **5a** (ΔE_{HL} = 2.17 V) are considerably larger than those reported for the acetylene- and butadiyne-linked zinc porphyrin dimers (ΔE_{HL} = 1.75−1.91 V).[24−26] These data imply that the π-conjugation between the two zinc porphyrin π-systems through the C−M−C linkages certainly operates at the one-electron oxidized state but is weak as compared to that through the acetylene-based π-spacers.

To get some insight into the degree of electronic communication through the C−M−C linkages at the oxidized states, we next performed spectroelectrochemical measurements for the π-radical monocations and dications of phospha-metallacycle-fused porphyrin dimers, generated from **3a**, **4a**, and **5a** in CH_2Cl_2 in the presence of Bu_4NPF_6 (Figure 4d−f).[27] The spectral changes were monitored at several intervals by using an optically transparent thin-layer electrochemical cell. As mentioned above, the bis(μ-acetato)-bridged zinc porphyrin dimer **4a** displayed one-step, 2e-oxidation for the first oxidation process in CV and DPV. In fact, during the progress of the oxidation from **4a** to **4a**$^{2+}$, the Soret and Q bands of the neutral species decreased and new broad absorption bands appeared constantly at around 600−740 nm with isosbestic points at 415, 452, 540, and 570 nm (Figure 4e). The new low-energy absorptions are likely due to the porphyrin π-radical dications (**4a**$^{2+}$),[28] which represents that the two porphyrin subunits are oxidized simultaneously. In this regard, **4a** should be classified by a localized system (class I system).[29]

In contrast, the Pd-linked dimer **3a** and the Pt-linked dimer **5a** showed stepwise spectral changes during the electrochemical oxidation, which are rationalized by considering the generation of 1e-oxidized π-radical monocation intermediates (Figure 4d,f). In the first 1e-oxidation step from **3a** to **3a**$^{+\bullet}$ the Soret band was slightly sharpened, and, in the following 1e-oxidation step from **3a**$^{+\bullet}$ to **3a**$^{2+}$, the Soret band split into two peaks with decreasing intensity (Figure 4d). After the 2e-oxidation, new Q-like bands that are characteristics of porphyrin π-radical cations appeared as broad absorption bands at around 650 nm. Although the whole spectral features differ from those of **3a**, the Pt-linked dimer **5a** also showed stepwise spectral changes during the electrochemical oxidation (Figure 4f). In the first 1e-oxidation step from **5a** to **5a**$^{+\bullet}$, the broad absorptions at 450−500 nm diminished, and, in the following 1e-oxidation step from **5a**$^{+\bullet}$ to **5a**$^{2+}$, the Soret-like bands decreased in intensity and new Q bands appeared at around 650 nm, as was observed for **3a**. It should be noted here that no intervalence charge-transfer band was detected at the near IR region (1000−2500 nm) during the electrochemical oxidation processes in the present diporphyrin π-systems. This implies that the interporphyrin electronic communication through the C−M−C linkages in **3a**$^{+\bullet}$ and **5a**$^{+\bullet}$ is considerably weaker than that provided by the acetylene-based bridges.[23,25] Consequently, the π-radical cations **3a**$^{+\bullet}$ and **5a**$^{+\bullet}$ can be better classified by a class II system that is exceedingly close to class I.

5. Theoretical Studies. To shed light on the nature of the dπ−pπ orbital interaction of the C−M−C linkages as well as its influences on the optical properties of the diporphyrin π-systems, DFT calculations of the *meso*-phenyl-substituted derivatives **3c** and **5c** were reperformed at the B3LYP level by using the Christiansen's basis set with the effective core potential (ECP) for Pd and Pt atoms and cc-pVDZ basis sets for H, C, N, and P atoms.[30] The electronic structure and excitation energies of porphyrin monomer reference 2c were also calculated at the same level. Except for hydrogen, the initial geometries of **3c** and **5c** were taken to be the same as the experimentally characterized geometries of **3b** and **5a** for the geometry optimization. In the time-dependent DFT (TD−DFT) calculations of the vertical excited states, the solvent effects of toluene were included using a polarizable continuum model (PCM) method. Further computational details are described in the Experimental Section.

dx.doi.org/10.1021/ja210205v | *J. Am. Chem.Soc.* 2012, 134, 1825−1839

Top and side views of the optimized structures of **2c**, **3c**, and **5c** are shown in Figure 5, and selected bond lengths and angles

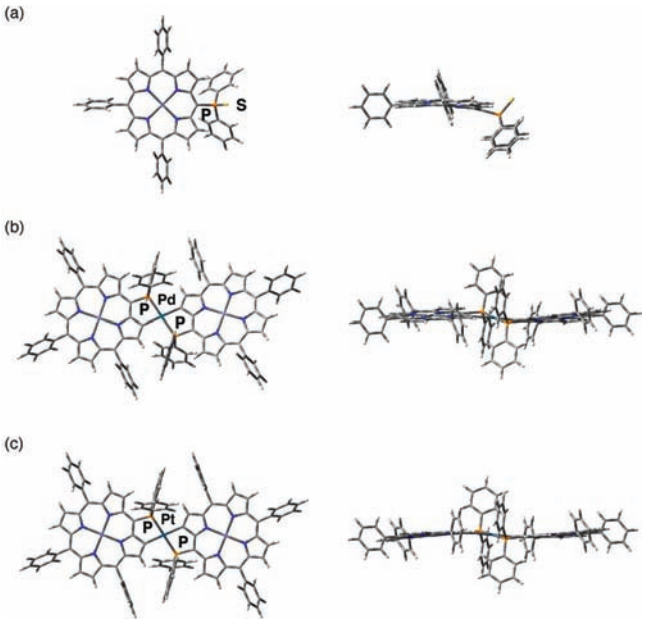

Figure 5. Top and side views of (a) **2c**, (b) **3c**, and (c) **5c** optimized by the B3LYP method.

are listed in Table S3 in the Supporting Information. The π-plane of **2c** is distorted to avoid the steric repulsion with the thiophosphoryl group. The palladium and platinum centers adopt a square planar geometry with the inside C−M−P (M = Pd, Pt) bond angles of 80.0−80.6 Å. In each complex, the metal-linked two porphyrin π-planes are slightly ruffled probably due to the steric effect of the fused metallacycle units. The porphyrin π-planes in **3c** are rather twisted at the phosphametallacycle linkages as compared to those in **5c**. The Pd−C bond lengths of **3c** (2.083−2.085 Å)[31] are almost identical to the sum of covalent-bond radii of palladium and carbon (ca. 2.07 Å),[32] implying that the Pd−C bonds in **3c** possess only a weak multiple bond character due to the metal-to-carbon π back-donation. The average Pt−C bond length of **5c** (2.076 Å) is also close to the sum of their covalent-bond radii (ca. 2.08 Å). As a consequence, the Zn−Zn distance between the two porphyrin centers of **3c** (12.31 Å) is almost the same as those of **5c** (12.30 Å). These structural features indicate that the differences in the absorption properties between **3c** and **5c** basically stem from the different C−M−C bonding interaction between these two compounds.

The molecular orbital diagrams of the selected orbitals at the optimized structures of **2c**, **3c**, and **5c** are summarized in Figures 6, 7, and 8, respectively. The excitation energies and their assignments calculated by the TD−DFT method are listed in Table 3. As shown in Figure 6, the attachment of the electron-withdrawing and bulky thiophosphoryl group at the *meso* position causes distortion of the porphyrin π-system and stabilization of LUMO compared to LUMO+1. In the high-energy excitations of **2c**, the lone electron pairs of sulfur (HOMO−2 and HOMO−3) are included as major components. The theoretically calculated excitation energy of the most intense Soret band of **2c** in toluene (406 nm) is larger by 0.2 eV than the observed one (λ_{max} = 433 nm).

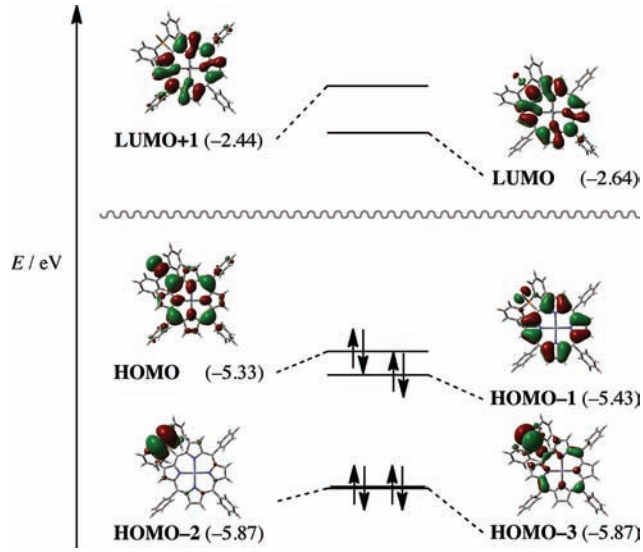

Figure 6. Molecular orbitals of **2c** and their energies (in eV) calculated by the B3LYP method in the gas phase.

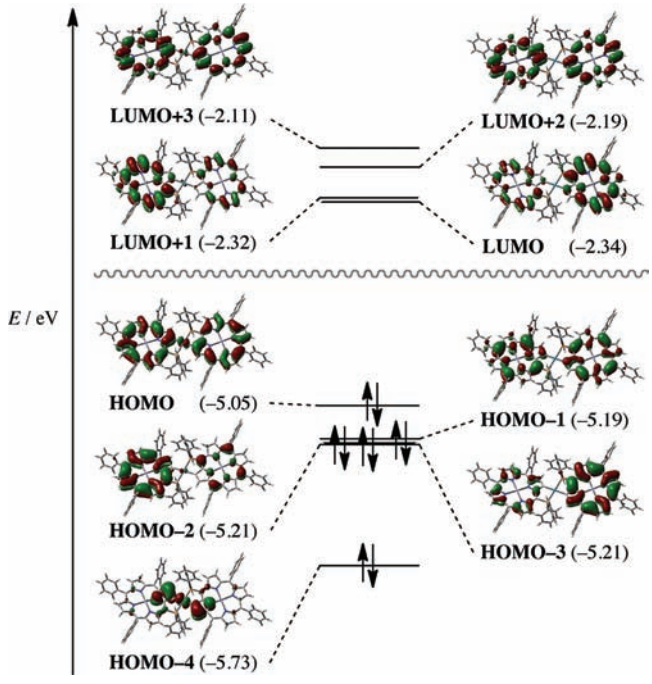

Figure 7. Molecular orbitals of **3c** and their energies (in eV) calculated by the B3LYP method in the gas phase.

As shown in Figures 7 and 8, eight orbitals from HOMO−3 to LUMO+3 of the metal-linked porphyrin dimers **3c** and **5c** are basically linear combinations of typical four orbitals (HOMO−1, HOMO, LUMO, LUMO+1) of each porphyrin ligand. In both dimers, however, HOMO is appreciably destabilized compared to HOMO−1, owing to the antibonding interaction between the metal (Pd, Pt) dπ orbital and the pyrrolic pπ orbital. The energy difference between HOMO and HOMO−1 of **5c** (0.20 eV) is larger than that of **3c** (0.14 eV), suggesting that the dπ−pπ orbital interaction in the C−Pt−C linkage is more prominent than that in the C−Pd−C linkage. Furthermore, the fact that the HOMO energy level of **5c** is higher than that of **3c** correlates well with the CV/DPV observations; **5a** ($E_{ox,1}$ = 0.31 V) was easier to oxidize than **3a**

dx.doi.org/10.1021/ja210205v | *J. Am. Chem.Soc.* 2012, 134, 1825−1839

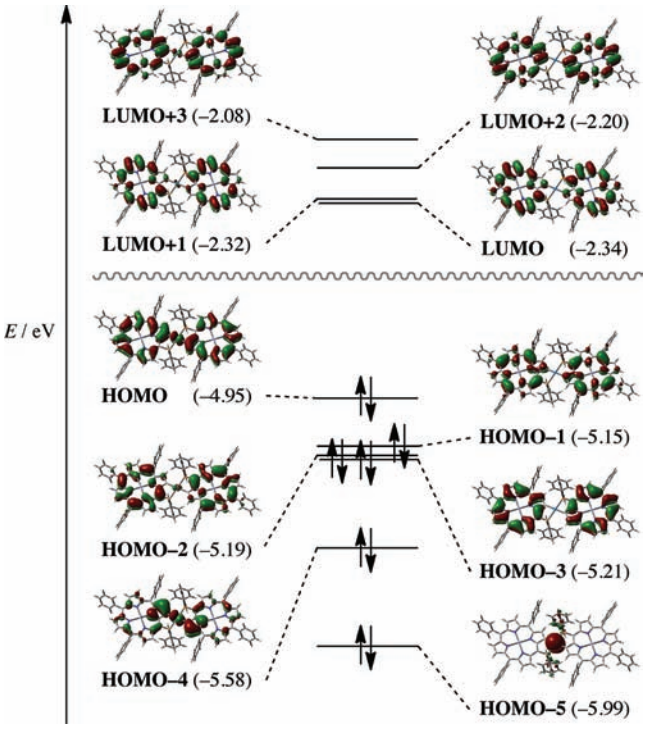

Figure 8. Molecular orbitals of **5c** and their energies (in eV) calculated by the B3LYP method in the gas phase.

($E_{ox,1}$ = 0.35 V). A similar antibonding dπ−pπ interaction is exhibited more clearly in HOMO−4s of **3c** and **5c**; HOMO−4 of **5c** (−5.58 eV) is less stabilized than HOMO−4 of **3c** (−5.73 eV). HOMOs and HOMO-4s exhibit the small contribution of dπ orbitals because of metal d orbitals existing at the low energy level compared to HOMO and HOMO−1 of a porphyrin monomer. The other frontier orbitals are almost at the same energy levels. As the difference in M−C bond lengths (M = Pd, Pt) is very small (Δd_{M-C} < 0.01 Å), the difference in the degree of the dπ−pπ orbital interaction between **3c** and **5c** can be attributed mainly to different orbital energies of square planar palladium(II) and platinum(II) atoms. To ensure this interpretation, we performed DFT calculations on *trans*-$PdR_2(PH_3)_2$ and *trans*-$PtR_2(PH_3)_2$ (R = Me or 3-pyrrolyl) as simplified models for evaluating the relative energy levels of the frontier dπ orbitals as well as their effects on the dπ−pπ orbital interaction. The results are summarized in Figure S6 in the Supporting Information. In *trans*-$MMe_2(PH_3)_2$, HOMO−2 (M = Pd) and HOMO−1 (M = Pt) are substantial dπ orbitals of palladium(II) or platinum(II). It is obvious that the dπ orbital of platinum(II) is located at the high energy level compared to that of palladium(II). In *trans*-$M(3\text{-pyrrolyl})_2(PH_3)_2$, each HOMO consists of the metal-derived dπ orbital and the pyrrole-derived pπ orbital and is destabilized compared to the purely pyrrole-based pπ orbital (HOMO−1). It should be mentioned that the destabilization energy calculated for the Pt model ($E_{HOMO} - E_{HOMO-1}$ = 0.46 eV) is larger than that calculated for the Pd model ($E_{HOMO} - E_{HOMO-1}$ = 0.37 eV), which correlates well with the above-mentioned DFT results on **3c** and **5c**. HOMO−7s are substantial dπ orbitals of palladium(II) or platinum(II) and show that the dπ orbital of platinum(II) is located at the high energy level compared to that of palladium(II). Accordingly, the energy difference between metal dπ and porphyrin π orbitals for the Pd model becomes larger than that for the Pt model. These results indicate that the porphyrin- or pyrrole-based pπ orbital can interact with the high-lying platinum(II) dπ orbital more strongly than the low-lying palladium(II) dπ orbital because of the relatively small energy difference between the two orbitals.

The simulated spectra of **3c** and **5c** do not completely match the experimentally observed ones of **3c** and **5c** in terms of excitation energies; however, the split excitations at the Soret-band regions of **3c** and **5c** are qualitatively consistent with the observed results obtained by absorption spectroscopy. It is noteworthy that the excited electron configuration at 400−430 nm

Table 3. Excitation Energies and Oscillator Strengths of 2c, 3c, and 5c Calculated by the TD-B3LYP Method with Solvation Effects[a]

		excitation energy				
	state	eV	nm	oscillator strength	excitation	weight (%)
2c	1	2.21	560	0.06	HOMO → LUMO	32.8
					HOMO-1 → LUMO+1	18.1
	3	2.79	444	0.30	HOMO-2 → LUMO	35.7
	5	2.95	421	0.63	HOMO-3 → LUMO	17.0
	6	3.06	406	1.08	HOMO-1 → LUMO+1	14.6
					HOMO-2 → LUMO	10.4
	7	3.18	390	0.54	HOMO-2 → LUMO+1	37.4
3c	1	2.25	557	0.09	HOMO → LUMO	12.7
					HOMO → LUMO+1	10.9
	9	2.65	468	0.56	HOMO → LUMO+2	23.1
					HOMO−1 → LUMO+3	11.7
	13	2.88	431	0.49	HOMO−4 → LUMO	18.9
					HOMO−3 → LUMO+3	15.8
	15	2.97	418	1.91	HOMO−4 → LUMO	10.2
	17	3.09	401	1.06	HOMO−4 → LUMO+2	27.6
	20	3.13	396	1.86	HOMO−4 → LUMO	8.1
5c	1	2.18	569	0.23	HOMO → LUMO	37.6
	7	2.54	488	0.82	HOMO → LUMO+2	18.9
					HOMO−1 → LUMO+1	13.6
	15	2.93	423	0.59	HOMO−4 → LUMO+2	19.1
					HOMO−3 → LUMO+3	14.1
	17	3.05	407	2.30	HOMO−4 → LUMO+2	20.1
	19	3.11	399	0.85	HOMO−5 → LUMO	26.3
	20	3.13	396	1.85	HOMO−5 → LUMO	13.2

[a]The states whose excitation energies are more than 3.20 eV or whose oscillator strengths are less than 0.30 are not included except for Q bands.

dx.doi.org/10.1021/ja210205v | J. Am. Chem.Soc. 2012, 134, 1825−1839

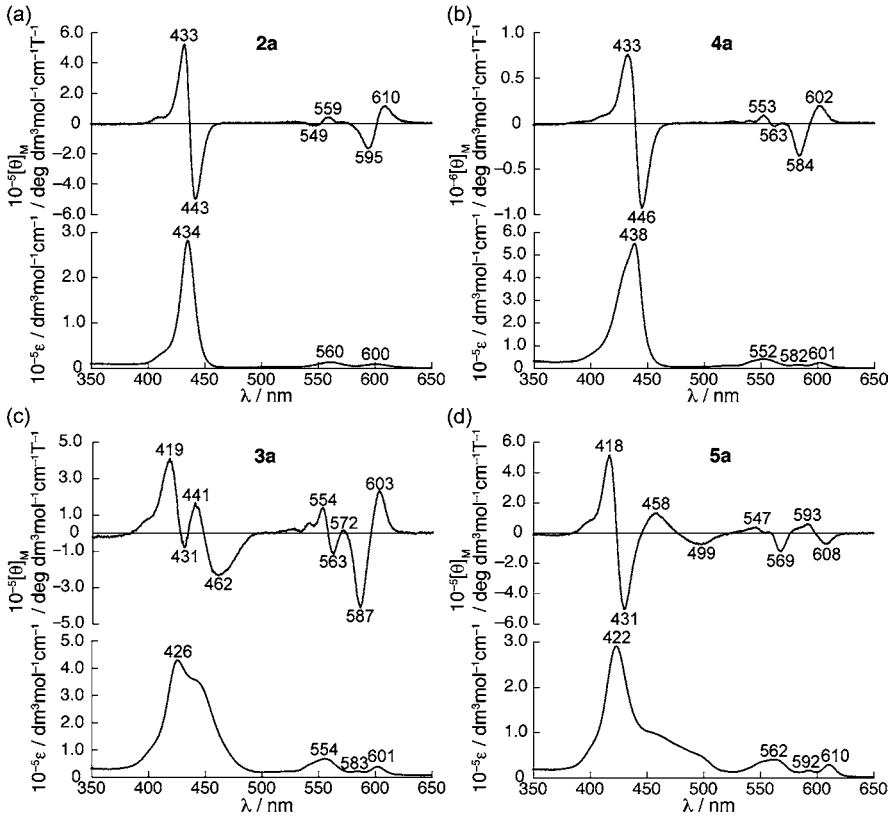

Figure 9. UV−vis absorption (bottom) and MCD (top) spectra of (a) **2a**, (b) **4a**, (c) **3a**, and (d) **5a** in toluene.

calculated for **3c** and **5c** include the electronic transitions from the respective HOMO−4s. This accounts for a possible contribution of the dπ−pπ orbital interaction to the absorption properties of the metal-linked coplanar phosphametallacycle-fused porphyrin dimers. The difference in the first excitation energies of **3c** (2.25 eV) and **5c** (2.18 eV) reflects their HOMO−LUMO gaps, namely the degree of dπ−pπ mixing in HOMO. In the high-energy (>3.1 eV) excitations of **5c**, the other low-lying Pt-derived d orbital (HOMO−5) is also involved.

6. Magnetic Circular Dichroism Spectroscopy. As mentioned above, the absorption spectra of **3a−c** and **5a** display intense Soret bands and relatively weak Q bands at almost the same regions observed for the respective porphyrin monomers **2a−c**. In this context, the present phosphametallacycle-linked porphyrin dimers are regarded as weakly π-conjugating systems, wherein the dipole−dipole interaction between the two isolated chromophores may be dominant. However, the unusually broadened and/or split absorptions at around 450−500 nm, as well as the split oxidation potentials observed for **3a** and **5a** cannot be rationalized by taking only the dipole−dipole interaction into consideration. To get deeper insight into the origin of the splitting/broadening of the Soret bands of the metal-linked porphyrin dimers **3** and **5** as well as understanding whether or not the through-bond pπ−dπ orbital interaction at the C−M−C linkages induces their unusual spectral properties, we finally carried out magnetic circular dichroism (MCD) measurements of **2a**, **3a**,**b**, **4a**, and **5a** in toluene (Figure 9). MCD spectroscopy has provided valuable information about ground- and excited-state degeneracy of macrocyclic π-conjugation systems, which is beneficial for understanding the electronic structure−spectra correlations of porphyrin chromophores.[33]

The MCD signals of the porphyrin monomer **2a** appeared as dispersion-type pseudo-Faraday *A* terms corresponding to the absorption peaks in both the Soret-band and Q-band regions (Figure 9a). As a 3-fold or higher symmetry axis is lacking for **2a**, however, this spectral pattern should be basically interpreted as superimposition of closely lying Faraday *B* terms, which is conventionally referred to as a pseudo Faraday *A* term. The changes in the sign of the MCD patterns in the Q-band and Soret-band regions are plus-to-minus and minus-to-plus, respectively, on going from the longer to shorter wavelengths. In general, the MCD signal patterns of the porphyrin monomers reflect the difference in splitting energies between ΔHOMO ($E_{HOMO} - E_{HOMO-1}$) and ΔLUMO ($E_{LUMO+1} - E_{LUMO}$); in the case of ΔHOMO > ΔLUMO, the MCD sign changes from minus to plus, whereas in the case of ΔHOMO < ΔLUMO, it changes from plus to minus. Because of the attachment of the *meso*-thiophosphoryl group, both HOMOs and LUMOs of **2a** are nondegenerate, as indicated in section 5. The observed MCD spectrum of **2a** implies that ΔLUMO is larger than ΔHOMO, because the MCD signal pattern of the Q region would be more sensitive to the difference between ΔHOMO and ΔLUMO than that of the Soret band region. The opposite sign pattern (plus-to-minus in the Q region and minus-to-plus in the Soret region) observed for **2a** may be attributable to a small difference between ΔHOMO and ΔLUMO of this compound,[34] which is consistent with the theoretical prediction for **2c**; ΔLUMO (0.20 eV) is only slightly larger than ΔHOMO (0.10 eV).

The MCD spectrum of **4a** is similar to that of **2a**; the sign changes from plus (602 nm) to minus (584 nm) in the low-energy Q-band region and from minus (446 nm) to plus (433 nm) in the Soret band region (Figure 9b). This indicates

dx.doi.org/10.1021/ja210205v | *J. Am. Chem.Soc.* 2012, 134, 1825−1839

that the introduction of the PdOAc group at the pyrrolic β position does not significantly perturb the character of excitations and the difference in splitting energies (ΔHOMO vs ΔLUMO) of the phosphanylporphyrin chromophore. The relatively broad and unsymmetrical Soret band observed in the absorption spectrum of **4a** may stem from weak exciton coupling, namely a dipole−dipole interaction at the excited state between the spatially separated chromophores.

In contrast, the whole spectral features of **3a** differ considerably from those of **2a** and **4a**. In the MCD spectrum of **3a** (Figure 9c), two Faraday *B* terms were detected at 462 nm (minus) and 441 nm (plus), whereas a dispersion-type pseudo-Faraday *A* term corresponding to the sharp Soret-like absorption was observed at ca. 420 nm. The MCD spectra of **3a**,**b** are very close to each other, as expected from the observations of their absorption spectra. Similarly, the MCD spectrum of **5a** exhibited minus-to-plus Faraday *B* terms at 499 and 458 nm (Figure 9d). Despite the difference in shapes of the absorption spectra in the Soret band region between **3a** and **5a**, the appearance of the *B* terms at the low-energy region by linking two porphyrin chromophores with palladium or platinum implies the same origin of these magnetically coupled MCD signals. The TD−DFT calculations of **3c** suggest that the absorption bands around this region (418 and 430 nm) involve the HOMO−4-to-LUMO transition as a major component (ca. 20% in weight) as well as $\pi-\pi^*$ transitions, i.e., transitions from the HOMO−1 to HOMO−3 to the LUMOs (each, ca. ∼10% in weight). It appears most probable that these porphyrin-based $\pi-\pi^*$ transitions mainly contribute to the MCD signals at around 450 nm since the change of angular momentum in the HOMO−4-to-LUMO transition *per se* is probably small. It was also reported, however, that in the absorption spectra of alkoxy- and alkylthio-substituted phthalocyanines,[35] the absorptions corresponding to basically forbidden n−π^* transitions (n: nonbonding orbital of oxygen or sulfur) were intensified by interstate mixing with the high-energy $\pi-\pi^*$ transitions (Soret band).[36] The appearance of the new absorption and the intense MCD signals for the present dimers can also be interpreted by considering a similar interstate-mixing between the intrinsically weak, *d*-orbital-derived transitions (for example, HOMO−4-to-LUMO) and the symmetrically allowed porphyrin $\pi-\pi^*$ transitions through the C−M−C linkage (M = Pd, Pt). Slight differences in the contribution of these two types of transitions can result in changes in the positions of the absorption bands (450 and 470 nm) and the MCD intensities of **3a** and **5a**.

In the Q-band region, the sign of the MCD signals observed for Pt-linked dimer **5a** is opposite to that observed for the Pd-linked dimer **3a**; the former changes from minus (608 nm) to plus (593 nm), whereas the latter changed from plus (603 nm) to minus (587 nm). This indicates that the MCD signals corresponding to the Q bands of **3a** and **5a** are also highly sensitive to the peripheral C−M−C linkages. Indeed, energetic differences between the theoretically calculated ΔHOMO (from HOMO to HOMO−3) and ΔLUMO (from LUMO to LUMO+3) for **3c** and **5c** are very small; ΔLUMO is larger than ΔHOMO by 0.07 eV for **3c**, whereas ΔHOMO is almost the same as ΔLUMO for **5c**. It is now evident that the peripheral C−M−C linkages (M = Pd, Pt) weakly but definitely affect the electronic structures as well as orbital energies of the adjacent diporphyrin π-systems through the dπ−pπ orbital interaction.

CONCLUSIONS

A new class of metal-linked, coplanar porphyrin dimers have been successfully constructed by the reaction of *meso*-(diphenylphosphanyl)porphyrins with palladium(II) and platinum(II) salts, in which the P−M coordination and the regioselective C−H activation (C−M bond formation) occur sequentially to fuse phosphametallacycles into the periphery. Both the experimental (steady-state and transient UV−vis absorption/fluorescence spectroscopy, CV, DPV, spectroelectrochemical measurements, and MCD spectroscopy) and theoretical (DFT and TD−DFT calculations) studies have disclosed that the linear C−M−C (M = Pd, Pt) linkages play intriguing roles in providing the characteristic optical, photophysical, and electrochemical properties of this class of coplanar diporphyrin π-systems. It is worth noting that the dπ−pπ orbital interaction at the C−M−C linkages weakly but definitely affects the reciprocal electronic communication between the porphyrin rings. For instance, this antibonding orbital interaction destabilizes the highest occupied molecular orbitals of the adjacent porphyrin π-systems and produces the unique absorption properties of the porphyrin chromophores. Additionally, the C−Pt−C linkage makes more significant impacts on their electronic coupling than does the C−Pd−C linkage. It should be emphasized again that the present C−M−C linkages connect two porphyrin π-systems in a coplanar fashion and within a short center-to-center distance. These structural features could be advantages in case the intrinsic electrochemical properties of each porphyrin component should be largely preserved or finely tuned in densely connected multiporphyrin arrays. The fundamental information obtained in this study will be helpful for the rational design of conceptually new supramolecular porphyrin architectures based on the peripheral metal−carbon bonds.

EXPERIMENTAL SECTION

General Remarks. ^{1}H and ^{31}P NMR spectra were recorded on a JEOL JNM-EX400 or JEOL JNM-AL300 spectrometer using $CDCl_3$ or CD_2Cl_2 as a solvent. Chemical shifts are reported in ppm as relative values vs tetramethylsilane (internal reference for ^{1}H) and 85% phosphoric acid (external reference for ^{31}P). The ^{1}H NMR spectra of new compounds are shown in Figures S6−S9 in the Supporting Information. Matrix-assisted laser desorption/ionization (MALDI) time-of-flight mass spectra (TOF) were measured on a SHIMADZU Biotech AXIMA-CFR spectrometer using α-cyano-4-hydroxycinnamic acid (CHCA) as a matrix. UV−vis absorption spectra were measured on a PerkinElmer Lambda 900 UV/vis/NIR spectrometer. Steady-state fluorescence spectra were recorded with a SPEX Fluoromax-3 spectrofluorometer (HORIBA). The solvents used for the reactions were distilled from sodium benzophenone ketyl (THF) or calcium hydride (CH_2Cl_2) under inert atmosphere before use. Other chemicals and solvents were of reagent grade quality, purchased commercially, and used without further purification. Thin-layer chromatography and flash column chromatography were performed with Alt. 5554 DC-Alufolien Kieselgel 60 F_{254} (Merck) and Silica-gel 60N (Kanto Chemicals), respectively. All reactions were performed under an argon atmosphere unless otherwise noted. The syntheses and spectral data of the *meso*-phenyl-substituted derivatives **1c**, **2c**, **3c**, and **5c** are described below, and those of the remaining compounds were reported in the Supporting Information of ref 5.

Synthesis of 2c. A 50 mL flask containing [5-iodo-10,15,20-triphenylporphyrinato]zinc[37] (90 mg, 0.12 mmol) and $Pd(OAc)_2$ (5.5 mg, 0.025 mmol) was evacuated in vacuo and then filled with argon. The same manipulation was carried out three times. THF (24 mL), MeCN (16 mL), triethylamine (68 μL, 0.49 mmol), and diphenylphosphine (43 μL, 0.25 mmol) were added via syringes to

dx.doi.org/10.1021/ja210205v | J. Am. Chem.Soc. 2012, 134, 1825−1839

the flask, and the resulting mixture was stirred at 80 °C for 11 h. After checking the consumption of the iodoporphyrin by TLC, S_8 (7.8 mg, 0.031 mmol) was added to the mixture. After 0.5 h, the mixture was filtered through a Celite bed, and the filtrate was concentrated under reduced pressure to leave a solid residue, which was then chromatographed on silica gel using hexane, CH_2Cl_2, and AcOEt as eluents. The bluish purple fraction (R_f = 0.22 in hexane/AcOEt = 5/1) was collected, concentrated, and recrystallized from CH_2Cl_2/MeOH to give **2c** as a purple solid (93 mg, 92%). ^{1}H NMR (400 MHz, CD_2Cl_2): δ 7.30 (m, 4H; P−Ph), 7.41 (m, 2H; P−Ph), 7.68−7.85 (m, 13H; *meso*-Ph, P−Ph), 8.07 (d, 4H, J = 8.0 Hz; *meso*-Ph), 8.18 (d, 2H, J = 8.0 Hz; *meso*-Ph), 8.45 (d, 2H, J = 4.8 Hz; β-H), 8.75 (d, 2H, J = 4.4 Hz; β-H), 8.83 (d, 2H, J = 4.4 Hz; β-H), 9.10 (d, 2H, J = 4.8 Hz; β-H). ^{31}P NMR (162 MHz, $CDCl_3$): δ 39.8. MS (MALDI−TOF): m/z 819 ([M + H]$^+$, 100%). UV−vis (toluene): λ_{max} (ε) 433 (336000), 559 (15800), 598 nm (10600 M^{-1} cm^{-1}).

Synthesis of 1c. A 50 mL flask containing **2c** (150 mg, 0.183 mmol) was evacuated in vacuo and then filled with argon. The same manipulation was carried out three times. Toluene (60 mL) and tris(dimethylamino)phosphine (2.3 mL, 13 mmol) were added via syringes to the flask, and the resulting mixture was stirred at 130 °C. After 5 h, **2c** was consumed completely (checked by TLC). The solvent was concentrated under reduced pressure to leave a solid, which was recrystallized from CH_2Cl_2/MeOH under argon atmosphere to give **1c** as a purple solid (137 mg, 95%). ^{1}H NMR (400 MHz, $CDCl_3$): δ 7.22−7.25 (m, 6H; P−Ph), 7.61−7.33 (13H; *meso*-Ph, P−Ph), 8.15−8.19 (6H; *meso*-Ph), 8.75 (d, 2H, J = 4.8 Hz; β-H), 8.77 (d, 2H, J = 4.4 Hz; β-H), 8.83 (d, 2H, J = 4.8 Hz; β-H), 9.82 (d, 2H, J = 4.8 Hz; β-H). ^{31}P NMR (162 MHz, $CDCl_3$): δ −5.5.

Synthesis of 3c. A mixture of **1c** (30 mg, 0.038 mmol), $Pd(OAc)_2$ (7.1 mg, 0.032 mmol), and toluene (10 mL) was stirred at room temperature in the dark for 0.5 h. The mixture was concentrated under reduced pressure to leave a solid residue, which was chromatographed on silica gel using hexane/CH_2Cl_2 as eluents. The reddish orange fraction (R_f = 0.52 in hexane/AcOEt = 5/2) was collected, concentrated, and reprecipitated from CH_2Cl_2/MeOH to give **3c** as a reddish purple solid (22 mg, 74%). ^{1}H NMR (400 MHz, CD_2Cl_2): δ 7.16 (t, 8H, J = 7.6 Hz; P−Ph), 7.26 (t, 4H, J = 7.6 Hz; P−Ph), 7.66−7.69 (m, 12H; *meso*-Ph), 7.75 (t, 4H, J = 7.6 Hz; *meso*-Ph), 7.86 (t, 2H, J = 7.6 Hz; *meso*-Ph), 8.07−8.21 (m, 20H; *meso*-Ph, P−Ph), 8.63 (d, 2H, J = 4.4 Hz; β-H), 8.67 (d, 2H, J = 4.4 Hz; β-H), 8.70 (d, 2H, J = 4.4 Hz; β-H), 8.72 (d, 2H, J = 4.4 Hz; β-H), 8.75 (d, 2H, J = 5.2 Hz; β-H), 8.80 (s, 2H; β-H), 8.87 (d, 2H, J = 5.2 Hz; β-H). ^{31}P{^{1}H} NMR (162 MHz, $CDCl_3$): δ 48.3. MS (FAB): m/z 1676 ([M + H]$^+$, 100%). UV−vis (toluene): λ_{max} (ε) 423 (165000), 555 (23400), 583 (6900), 600 nm (12100 M^{-1} cm^{-1}).

Synthesis of 5c. A mixture of **1c** (17.6 mg, 0.0223 mmol), $PtCl_2$(cod) (4.2 mg, 0.011 mmol), and CH_2Cl_2 (5 mL) was stirred at room temperature in the dark for 2.5 h. The mixture was concentrated under reduced pressure to leave a solid residue, which was chromatographed on silica gel using CH_2Cl_2 as an eluent. The brown fraction (R_f = 0.17 in hexane/AcOEt = 5/1) was collected, concentrated, and reprecipitated from CH_2Cl_2/MeOH to give **5c** as a brownish purple solid (7.1 mg, 36%). ^{1}H NMR (400 MHz, CD_2Cl_2): δ 7.30 (t, 8H, J = 7.6 Hz; P−Ph), 7.40 (t, 4H, J = 7.3 Hz; P−Ph), 7.73−7.80 (m, 12H; *meso*-Ph, P−Ph), 7.84 (t, 4H, J = 7.6 Hz; *meso*-Ph), 7.95 (t, 2H, J = 7.6 Hz; *meso*-Ph), 8.15−8.23 (m, 12H; *meso*-Ph), 8.29 (m, 8H; P−Ph), 8.82 (d, 2H, J = 4.4 Hz; β-H), 8.85 (d, 2H, J = 4.4 Hz; β-H), 8.87 (d, 2H, J = 4.4 Hz; β-H), 8.89 (s, 2H; β-H), 8.90 (d, 2H, J = 4.8 Hz; β-H), 8.92 (d, 2H, J = 4.8 Hz; β-H), 9.02 (d, 2H, J = 4.8 Hz; β-H). ^{31}P{^{1}H} NMR (162 MHz, $CDCl_3$): δ 44.1 (J_{P-Pt} = 2810 Hz). MS (FAB): m/z 1765 ([M + H]$^+$, 100%). UV−vis (toluene): λ_{max} (relative intensity) 421 (231000), 562 (30200), 592 (14400), 609 nm (20600).

Time-Resolved Fluorescence Measurements. Fluorescence decays of the samples in the nanosecond and subnanosecond time scales were measured using a time-correlated single photon counting (TCSPC) system (PicoQuant GmBH) consisting of PicoHarp 300 controller and PDL 800-B driver. The samples were excited with the pulsed diode laser head LDH-P-C-405B at 405 nm and fluorescence decays were measured at the wavelengths of emission maxima at 616−631 nm, depending on the sample. The signals were detected with a microchannel plate photomultiplier tube (Hamamatsu R2809U). The time resolution of the TCSPC measurements was about 60 ps (fwhm of the instrument response function).

Subpicosecond to nanosecond time-resolved transient absorption spectra were collected using a pump−probe technique. The femtosecond pulses of the Ti:sapphire generator were amplified by using a multipass amplifier (CDP-Avesta, Moscow, Russia) pumped by a second harmonic of the Nd:YAG Q-switched laser (model LF114, Solar TII, Minsk, Belorussia). All measurements were carried out at room temperature. The amplified pulses were used to generate a second harmonic (410 nm) for sample excitation (pump beam) and a white continuum for time-resolved spectrum detection (probe beam). An average of 100 pulses at 10 Hz repetition rate was used to improve the signal-to-noise ratio. The excitation energy was adjusted to the level when sample degradation can be neglected in the end of the measurements. The transient spectra were recorded by a charge-coupled device (CCD) detector coupled with a monochromator (Newton DU920N and Shamrock form Andor Technology Ltd., respectively) in the visible and near-infrared ranges. The wavelength range collected in this study was 470−760 nm. The typical response time of the instrument was 150 fs (fwhm). A global multiexponential fitting procedure was applied to process the data and the spectra were fitted by the 3-exponential decay model. The procedure takes into account the instrument time response function and the group velocity dispersion of the white continuum and allows one to calculate the decay time constants and dispersion-compensated transient absorption spectra as described previously.[21]

Up-conversion instrument (FOG-100, CDP Corp.) for time-resolved fluorescence was used to detect the fast processes with a time resolution of 100 fs. The primary Ti:sapphire generator (TiF-50, CDP Corp.) was pumped by Nd CW laser (Verdi-6, Coherent Inc.), and a second harmonic (420 nm) was used to excite the sample solution in a rotating cuvette. Emission from the sample was collected to a nonlinear crystal (NLC), where it was mixed with the so-called gate pulse, which was the laser fundamental. The signal was measured at a sum frequency of the gate pulse and the selected emission maximum of the sample (at 620 nm). The gate pulse was passed through a delay line so that it arrived at NLC at a desired time after sample excitation. Scanning through the delay line the emission decay curve of the sample was detected. Concentration of the samples was similar to that for the measurement of the transient absorption spectra with the pump−probe technique (Abs = ca. 0.4 at 410 nm).

In nanosecond flash-photolysis experiments, the samples were exited at 400 nm and the decay curves and transient components spectra of the long-living component, evidently the triplet state, were determined in the presence and absence of oxygen.

Computational Details. For metal elements, the effective core potentials (ECP) proposed by Christiansen's group[38] were used for Zn(up to 2p), Pd(up to 3d), and Pt(up to 4f), and (541/5511/211), (541/541/211), and (761/681/411) basis sets were used for the valence electrons of Pt, Pd, and Zn, respectively. For the other H, C, N, and P, the cc-pVDZ basis sets were used.[39] The geometry optimization was performed by the B3LYP[40] method with above basis sets without any geometrical constraints except for *trans*-$MR_2(PH_3)_2$ (M = Pd, Pt; R = Me, 3-pyrrolyl), and X-ray structures for **3b** and **5a** were used as initial geometries for **3c** and **5c**, respectively. After Hessian calculations were carried out, we confirmed that the optimized geometries were not in saddle but in stable points. As a result, the stable geometries of **2c**, **3c**, and **5c** became C_1 symmetry. The *trans*-$MR_2(PH_3)_2$ (M = Pd, Pt; R = Me, 3-pyrrolyl) were optimized with keeping square planar geometries by the B3LYP method. Although *trans*-$MMe_2(PH_3)_2$ are stable geometries in Hessian calculations, *trans*-$M(3\text{-pyrrolyl})_2(PH_3)_2$ have three imaginary modes. The Cartesian coordinates are summarized in Tables S1 and S2, and the calculated bond parameters are listed in Table S3 in the Supporting Information.

The excited states and oscillator strengths are evaluated by the TD-B3LYP method, where 40 excited states were solved. In the time-dependent DFT (TD−DFT) calculations of the vertical excited states,

the effect of toluene solvent was estimated by the polarizable continuum model (PCM) method.[41] All calculations were carried out with the Gaussian 03 package.[42] Molecular orbitals with the isovalue of 0.02 are drawn by the Gauss View 4. The PCM calculations indicate Soret bands of all the porphyrins shift to lower energy in toluene relative to that in vacuum.

Electrochemical and Spectroelectrochemical Measurements. Cyclic and differential pulse voltammograms were recorded with an ALS 630a electrochemical analyzer using a glassy carbon working electrode, a platinum wire counter electrode, and an Ag/Ag^+ [0.01 M $AgNO_3$, 0.1 M nBu_4NPF_6 (MeCN)] reference electrode. The potentials were calibrated against ferrocene/ferrocenium [E_{mid} = +0.20 V vs Ag/Ag^+; scan rate 20 mV s^{-1}]. Spectroelectrochemical measurements were carried out with a custom-made optically transparent thin-layer electrochemical (OTTLE) cell (light pass length = 1 mm) equipped with a platinum mesh, a platinum coil, and a silver wire as the working, the counter, and the pseudoreference electrodes, respectively. The absorption spectra were measured with a Perkin-Elmer Lambda 19 spectrometer, and the potential was applied with an ALS/chi electrochemical analyzer model 612A.

Magnetic Circular Dichroism Spectroscopy Measurements. Electronic absorption spectra were recorded on a JASCO V-570 spectrophotometer. Magnetic circular dichroism (MCD) spectra were recorded on a JASCO J-725 spectrodichrometer equipped with a JASCO electromagnet, which produces magnetic fields of up to 1.09 T (1 T = 1 T) with both parallel and antiparallel fields. The magnitudes were expressed in terms of molar ellipticity per tesla ($[\theta]_M$/deg dm^3 mol^{-1} cm^{-1} T^{-1}).

■ ASSOCIATED CONTENT

Ⓢ Supporting Information

Complete ref 42, some spectral and theoretical data, and ^1H NMR charts for new compounds. This material is available free of charge via the Internet at http://pubs.acs.org.

■ AUTHOR INFORMATION

Corresponding Author

E-mail: (Y.M.) matano@scl.kyoto-u.ac.jp; (H.L.) helge.lemmetyinen@tut.fi; (N.K.) nagaok@m.tohoku.ac.jp

■ ACKNOWLEDGMENTS

This work was partially supported by a Grant-in-Aid for Scientific Research on Innovative Areas (Nos. 20108007 and 21108511, "π-Space") from the Ministry of Education, Culture, Sports, Science and Technology, Japan and the Sumitomo Foundation. H.L. and N.T. thank the Academy of Finland for financial support: Both H.L. and H.I. thank the Strategic Japanese-Finnish Cooperative Program (JST, Tekes, and AF) for their valuable support. H.H. is grateful for a JSPS fellowship for young scientists. Y.M. thanks Prof. Yoshifumi Kimura (Kyoto University) for his valuable comments on the photophysical properties.

■ REFERENCES

(1) For selected reviews and handbooks, see: (a) Sanders, J. K. M.; Bampos, N.; Clyde-Watson, Z.; Darling, S. L.; Hawley, J. C.; Kim, H.-J.; Mak, C. C.; Webb, S. J. In *The Porphyrin Handbook*; Kadish, K. M., Smith, K. M., Guilard, R., Eds.; Academic Press: San Diego, CA, 2000; Vol. *3*, pp 3−48. (b) Chambron, J.-C.; Heitz, V.; Sauvage, J.-P. In *The Porphyrin Handbook*; Kadish, K. M., Smith, K. M., Guilard, R., Eds.; Academic Press: San Diego, CA, 2000; Vol. *6*, pp 1−42. (c) Sanders, J. K. M. In *The Porphyrin Handbook*; Kadish, K. M., Smith, K. M., Guilard, R., Eds.; Academic Press: San Diego, 2000; Vol. 3, pp 347−368. (d) Imamura, T.; Fukushima, K. *Coord. Chem. Rev.* **2000**, *198*, 133−156. (e) Wojaczyński, J.; Latos-Grażyński, L. *Coord. Chem. Rev.* **2000**, *204*, 113−171. (f) Swiegers, G. F.; Malefetse, T. J. *Chem. Rev.* **2000**, *100*, 3483−3537. (g) Burrell, A. K.; Officer, D. L.; Plieger, P. G.; Reid, D. C. W. *Chem. Rev.* **2001**, *101*, 2751−2796. (h) Harvey, P. D. In *The Porphyrin Handbook*; Kadish, K. M., Smith, K. M., Guilard, R., Eds.; Academic Press: San Diego, CA, 2003; Vol. *18*, pp 63−250. (i) Goldberg, I. *Chem. Commun.* **2005**, 1243−1254. (j) Scandola, F.; Chiorboli, C.; Prodi, A.; Iengo, E.; Alessio, E. *Coord. Chem. Rev.* **2006**, *250*, 1471−1496. (k) Lee, S. J.; Hupp, J. T. *Coord. Chem. Rev.* **2006**, *250*, 1710−1723. (l) Kobuke, Y.; Ogawa, K. *Bull. Chem. Soc. Jpn.* **2003**, *76*, 689−708. (m) Alessio, E.; Bouamaied, I.; Coskun, T.; Ercolani, G.; Flamigni, L.; Gunter, M. J.; Heitz, V.; Hupp, J. T.; Iengo, E.; Kobuke, Y.; Sauvage, J.-P.; Scandola, F.; Stulz, E. In *Struct. Bonding (Berlin)*; Alessio, E., Ed.; Springer-Verlag: Heidelberg, 2006; Vol. *121*. (n) Maeda, C.; Kamada, T.; Aratani, N.; Osuka, A. *Coord. Chem. Rev.* **2007**, *251*, 2743−2752. (o) Satake, A.; Kobuke, Y. *Org. Biomol. Chem.* **2007**, *5*, 1679−1691. (p) Beletskaya, I.; Tyurin, V. S.; Tsivadze, A. Y.; Guilard, R.; Stern, C. *Chem. Rev.* **2009**, *109*, 1659−1713. (q) Tsuda, A. *Bull. Chem. Soc. Jpn.* **2009**, *82*, 11−28. (r) Aratani, N.; Kim, D.; Osuka, A. *Acc. Chem. Res.* **2009**, *42*, 1922−1934. (s) Otsuki, J. *J. Porphyrins Phthalocyanines* **2009**, *13*, 1069−1081. (t) Drain, C. M.; Varotto, A.; Radivojevic, I. *Chem. Rev.* **2009**, *109*, 1630−1658. (u) DeVries, L. D.; Choe, W. *J. Chem. Crystallogr.* **2009**, *39*, 229−240. (v) Miyatake, T.; Tamiaki, H. *Coord. Chem. Rev.* **2010**, *254*, 2593−2602.

(2) A large number of papers have been published for this issue. For selected examples, see: (a) Fleischer, E. B.; Shachter, A. M. *Inorg. Chem.* **1991**, *30*, 3763−3769. (b) Drain, C. M.; Lehn, J.-M. *J. Chem. Soc., Chem. Commun.* **1994**, 2313−2315. (c) Hunter, C. A.; Sarson, L. D. *Angew. Chem., Int. Ed. Engl.* **1994**, *33*, 2313−2316. (d) Kobuke, Y.; Miyaji, H. *J. Am. Chem. Soc.* **1994**, *116*, 4111−4112. (e) Stibrany, R. T.; Vasudevan, J.; Knapp, S.; Potenza, J. A.; Emge, T.; Schugar, H. J. *J. Am. Chem. Soc.* **1996**, *118*, 3980−3981. (f) Yuan, H.; Thomas, L.; Woo, L. K. *Inorg. Chem.* **1996**, *35*, 2808−2817. (g) Slone, R. V.; Hupp, J. T. *Inorg. Chem.* **1997**, *36*, 5422−5423. (h) Funatsu, K.; Imamura, T.; Ichimura, A.; Sasaki, Y. *Inorg. Chem.* **1998**, *37*, 4986−4995. (i) Fan, J.; Whiteford, J. A.; Olenyuk, B.; Levin, M. D.; Stang, P. J.; Fleischer, E. B. *J. Am. Chem. Soc.* **1999**, *121*, 2741−2752. (j) Darling, S. L.; Mak, C. C.; Bampos, N.; Feeder, N.; Teat, S. J.; Sanders, J. K. M. *New J. Chem.* **1999**, *23*, 359−364. (k) Prodi, A.; Indelli, M. T.; Kleverlaan, C. J.; Scandola, F.; Alessio, E.; Gianferrara, T.; Marzilli, L. G. *Chem.—Eur. J.* **1999**, *5*, 2668−2679. (l) Sun, D.; Tham, F. S.; Reed, C. A.; Chaker, L.; Burgess, M.; Boyd, P. D. W. *J. Am. Chem. Soc.* **2000**, *122*, 10704−10705. (m) Fujita, N.; Biradha, K.; Fujita, M.; Sakamoto, S.; Yamaguchi, K. *Angew. Chem., Int. Ed.* **2001**, *40*, 1718−1721. (n) Tsuda, A.; Nakamura, T.; Sakamoto, S.; Yamaguchi, K.; Osuka, A. *Angew. Chem., Int. Ed.* **2002**, *41*, 2817−2821. (o) Furuta, H.; Ishizuka, T.; Osuka, A. *J. Am. Chem. Soc.* **2002**, *124*, 5622−5623. (p) Qian, D.-J.; Nakamura, C.; Ishida, T.; Wenk, S.-O.; Wakayama, T.; Takeda, S.; Miyake, J. *Langmuir* **2002**, *18*, 10237−10242. (q) Iengo, E.; Zangrando, E.; Minatel, R.; Alessio, E. *J. Am. Chem. Soc.* **2002**, *124*, 1003−1013. (r) Vinodu, M.; Stein, Z.; Goldberg, I. *Inorg. Chem.* **2004**, *43*, 7582−7584. (s) Hwang, I.-W.; Kamada, T.; Ahn, T. K.; Ko, D. M.; Nakamura, T.; Tsuda, A.; Osuka, A.; Kim, D. *J. Am. Chem. Soc.* **2004**, *126*, 16187−16198. (t) Iengo, E.; Zangrando, E.; Bellini, M.; Alessio, E.; Prodi, A.; Chiorboli, C.; Scandola, F. *Inorg. Chem.* **2005**, *44*, 9752−9762. (u) Aimi, J.; Nagamine, Y.; Tsuda, A.; Muranaka, A.; Uchiyama, M.; Aida, T. *Angew. Chem., Int. Ed.* **2008**, *47*, 5153−5156. (v) Kira, A.; Umeyama, T.; Matano, Y.; Yoshida, K.; Isoda, S.; Park, J. K.; Kim, D.; Imahori, H. *J. Am. Chem. Soc.* **2009**, *131*, 3198−3200. (w) Koepf, M.; Conradt, J.; Szmytkowski, J.; Wytko, J. A.; Allouche, L.; Kalt, H.; Balaban, T. S.; Weiss, J. *Inorg. Chem.* **2011**, *50*, 6073−6082 See also ref 1.

(3) (a) Darling, S. L.; Stulz, E.; Feeder, N.; Bampos, N.; Sanders, J. K. M. *New J. Chem.* **2000**, *24*, 261−264. (b) Stulz, E.; Maue, M.; Feeder, N.; Teat, S. J.; Ng, Y.-F.; Bond, A. D.; Darling, S. L.; Sanders, J. K. M. *Inorg. Chem.* **2002**, *41*, 5255−5268. (c) Stulz, E.; Scott, S. M.; Bond, A. D.; Otto, S.; Sanders, J. K. M. *Inorg. Chem.* **2003**, *42*, 3086−3096. (d) Stulz, E.; Scott, S. M.; Ng, Y.-F.; Bond, A. D.; Teat, S. J.; Darling, S. L.; Feeder, N.; Sanders, J. K. M. *Inorg. Chem.* **2003**, *42*, 6564−6574.

(e) Stulz, E.; Maue, M.; Scott, S. M.; Mann, B. E.; Sanders, J. K. M. *New J. Chem.* **2004**, *28*, 1066−1072.
(4) (a) Matano, Y.; Matsumoto, K.; Terasaka, Y.; Hotta, H.; Araki, Y.; Ito, O.; Shiro, M.; Sasasmori, T.; Tokitoh, N.; Imahori, H. *Chem.—Eur. J.* **2007**, *13*, 891−901. (b) Matano, Y.; Shinokura, T.; Matsumoto, K.; Imahori, H.; Nakano, H. *Chem. Asian J.* **2007**, *2*, 1417−1429.
(5) Matano, Y.; Matsumoto, K.; Nakao, Y.; Uno, H.; Sakaki, S.; Imahori, H. *J. Am. Chem. Soc.* **2008**, *130*, 4588−4589.
(6) Matano, Y.; Matsumoto, K.; Shibano, T.; Imahori, H. *J. Porphyrins Phthalocyanines* **2011**, *15*, 1172−1182.
(7) For pioneering studies, see: (a) DiMagno, S. G.; Lin, V. S.-Y.; Therien, M. J. *J. Am. Chem. Soc.* **1993**, *115*, 2513−2515. (b) DiMagno, S. G.; Lin, V. S.-Y.; Therien, M. J. *J. Org. Chem.* **1993**, *58*, 5983−5993. (c) Lin, V. S.-Y.; DiMagno, S. G.; Therien, M. J. *Science* **1994**, *264*, 1105−1111. (d) Fletcher, J. T.; Therien, M. J. *J. Am. Chem. Soc.* **2002**, *124*, 4298−4311.
(8) (a) Atefi, F.; Arnold, D. P. *J. Porphyrins Phthalocyanines* **2008**, *12*, 801−831. (b) Suijkerbuijk, B. M. J. M.; Klein Gebbink, R. J. M. *Angew. Chem., Int. Ed.* **2008**, *47*, 7396−7421.
(9) A few ferrocene-linked parallel and slipped porphyrin dimers have been reported. (a) Wang, H. J. H.; Jaquinod, L.; Nurco, D. J.; Vicente, M. G. H.; Smith, K. M. *Chem. Commun.* **2001**, 2646−2647. (b) Shoji, O.; Okada, S.; Satake, A.; Kobuke, Y. *J. Am. Chem. Soc.* **2005**, *127*, 2201−2210. (c) Jiao, L.; Courtney, B. H.; Fronczek, F. R.; Smith, K. M. *Tetrahedron Lett.* **2006**, *47*, 501−504. (d) Wang, H. J. H.; Jaquinod, L.; Olmstead, M. M.; Vicente, M. G. H.; Kadish, K. M.; Ou, Z.; Smith, K. M. *Inorg. Chem.* **2007**, *46*, 2898−2913.
(10) Direct β-mercuration and β-borylation of β-free porphyrins: (a) Smith, K. M.; Langry, K. C. *J. Chem. Soc. Chem. Commun.* **1980**, 217−218. (b) Smith, K. M.; Langry, K. C. *J. Chem. Soc., Chem. Commun.* **1981**, 283−284. (c) Smith, K. M.; Langry, K. C.; Minnetian, O. M. *J. Org. Chem.* **1984**, *49*, 4602−4609. (d) Sugiura, K.-i.; Kato, A.; Iwasaski, K.; Miyasaka, H.; Yamashita, M.; Hino, S.; Arnold, D. P. *Chem. Commun.* **2007**, 2046−2047. (e) Hata, H.; Shinokubo, H.; Osuka, A. *J. Am. Chem. Soc.* **2005**, *127*, 8264−8265.
(11) Oxidative addition of *meso*-C−Br bonds of *meso*-bromoporphyrins to zerovalent group 10 metals (Pd, Pt): (a) Arnold, D. P.; Sakata, Y.; Sugiura, K.; Worthington, E. I. *Chem. Commun.* **1998**, 2331−2332. (b) Arnold, D. P.; Healy, P. C.; Hodgson, M. J.; Williams, M. L. *J. Organomet. Chem.* **2000**, *607*, 41−50. (c) Hodgson, M. J.; Healy, P. C.; Williams, M. L.; Arnold, D. P. *J. Chem. Soc., Dalton Trans.* **2002**, 4497−4504. (d) Hartnell, R. D.; Edwards, A. J.; Arnold, D. P. *J. Porphyrins Phthalocyanines* **2002**, *6*, 695−707.
(12) β-(2-Pyridyl)-directed *meso*-C−H activation with Pt(II), Pd(II), or Ru(II) salts: (a) Yamaguchi, S.; Katoh, T.; Shinokubo, H.; Osuka, A. *J. Am. Chem. Soc.* **2007**, *129*, 6392−6393. (b) Yamaguchi, S.; Shinokubo, H.; Osuka, A. *Inorg. Chem.* **2009**, *48*, 795−797. (c) Shinokubo, H.; Osuka, A. *Chem. Commun.* **2009**, 1011−1021. (d) Yamaguchi, S.; Shinokubo, H.; Osuka, A. *J. Am. Chem. Soc.* **2010**, *132*, 9992−9993. (e) Yoshida, K.; Yamaguchi, S.; Osuka, A.; Shinokubo, H. *Organometallics* **2010**, *29*, 3997−4000.
(13) Hartnell, R. D.; Arnold, D. P. *Organometallics* **2004**, *23*, 391−399.
(14) Yamaguchi, S.; Katoh, T.; Shinokubo, H.; Osuka, A. *J. Am. Chem. Soc.* **2008**, *130*, 14440−14441.
(15) (a) Song, J.; Aratani, N.; Heo, J. H.; Kim, D.; Shinokubo, H.; Osuka, A. *J. Am. Chem. Soc.* **2010**, *132*, 11868−11869. (b) Song, J.; Aratani, N.; Shinokubo, H.; Osuka, A. *J. Am. Chem. Soc.* **2010**, *132*, 16356−16357.
(16) Arnold suggested the formation of a *moso*-phosphanylporphyrin as an intermediate in their synthesis of *meso*-phosphorylporphyrins. See: (a) Atefi, F.; Locos, B.; Senge, M. O.; Arnold, D. P. *J. Porphyrins Phthalocyanines* **2006**, *10*, 176−185. (b) Atefi, F.; McMurtrie, J. C.; Turner, P.; Duriska, M.; Arnold, D. P. *Inorg. Chem.* **2006**, *45*, 6479−6489.
(17) For example, see: (a) Haenel, M. W.; Jakubik, D.; Krüger, C.; Betz, P. *Chem. Ber.* **1991**, *124*, 333−336. (b) Frey, G. D.; Reisinger, C.-P.; Herdtweck, E.; Herrmann, W. A. *J. Organomet. Chem.* **2005**, *690*, 3193−3201. (c) Frey, G. D.; Schts, J.; Herdtweck, E.; Herrmann, W. A. *Organometallics* **2005**, *24*, 4416−4426. (d) Hu, J.; Lin, R.; Yip, J. H. K.; Wong, K.-Y.; Ma, D.-L.; Vittal, J. J. *Organometallics* **2007**, *26*, 6533−6543. (e) Hu, J.; Yip, J. H. K.; Ma, D.-L.; Wong, K.-Y.; Chung, W.-H. *Organometallics* **2009**, *28*, 51−59. (f) Hu, J.; Yip, J. H. K. *Organometallics* **2009**, *28*, 1093−1100.
(18) (a) Rahn, J. A.; Baltusis, L.; Nelson, J. H. *Inorg. Chem.* **1990**, *29*, 750−755. (b) Power, W. P.; Wasylishen, R. E. *Inorg. Chem.* **1992**, *31*, 2176−2183.
(19) Seybold, P. G.; Gouterman, M. *J. Mol. Spectrosc.* **1969**, *31*, 1−13.
(20) Tkachenko, N. V.; Rantala, L.; Tauber, A. Y.; Helaja, J.; Hynninen, P. H.; Lemmetyinen, H. *J. Am. Chem. Soc.* **1999**, *121*, 9378−9387.
(21) For example, see: (a) Bajema, L.; Gouterman, M.; Rose, C. B. *J. Mol. Spectrosc.* **1971**, *39*, 421−431. (b) Kurabayashi, Y.; Kikuchi, K.; Kokubun, H.; Kaizu, Y.; Kobayashi, H. *J. Phys. Chem.* **1984**, *88*, 1308−1310. (c) Osuka, A.; Nagata, T.; Kobayashi, F.; Zhang, R. P.; Maruyama, K.; Mataga, N.; Asahi, T.; Ohno, T.; Nozaki, K. *Chem. Phys. Lett.* **1992**, *199*, 302−308. (d) Chosrowjan, H.; Tanigichi, S.; Okada, T.; Takagi, S.; Arai, T.; Tokumaru, K. *Chem. Phys. Lett.* **1995**, *242*, 644−649.
(22) For example, see: (a) Le Mest, Y.; L'Her, M.; Hendricks, N. H.; Kim, K.; Collman, J. P. *Inorg. Chem.* **1992**, *31*, 835−847. (b) Kadish, K. M.; Guo, N.; Van Caemelbecke, E.; Froiio, A.; Paolesse, R.; Monti, D.; Tagliatesta, P.; Boschi, T.; Prodi, L.; Bolletta, F.; Zaccheroni, N. *Inorg. Chem.* **1998**, *37*, 2358−2365. (c) Anderson, H. L. *Chem. Commun.* **1999**, 2323−2330. (d) Frampton, M. J.; Akdas, H.; Cowley, A. R.; Rogers, J. E.; Slagle, J. E.; Fleitz, P. A.; Drobizhev, M.; Rebane, A.; Anderson, H. L. *Org. Lett.* **2005**, *7*, 5365−5368. (e) Fendt, L.-A.; Fang, H.; Plonska-Brzezinska, M. E.; Zhang, S.; Cheng, F.; Braun, C.; Echegoyen, L.; Diedrich, F. *Eur. J. Org. Chem.* **2007**, 4659−4673.
(23) Chen, Y.-J.; Chen, S.-S.; Lo, S.-S.; Huang, T.-H.; Wu, C.-C.; Lee, G.-H.; Peng, S.-M.; Yeh, C.-Y. *Chem. Commun.* **2006**, 1015−1017.
(24) (a) Richeter, S.; Jeandon, C.; Ruppert, R.; Callot, H. J. *Chem. Commun.* **2001**, 91−92. (b) Richeter, S.; Jeandon, C.; Gisselbrecht, J.-P.; Ruppert, R.; Callot, H. J. *J. Am. Chem. Soc.* **2002**, *124*, 6168−6179.
(25) Huang, T.-H.; Chen, Y.-J.; Lo, S.-S.; Yen, W.-N.; Mai, C.-L.; Kuo, M.-C.; Yeh, C.-Y. *Dalton Trans.* **2006**, 2207−2213.
(26) (a) Arnold, D. P.; Heath, G. A.; James, D. A. *New J. Chem.* **1998**, 1377−1387. (b) Arnold, D. P.; Hartnell, R. D.; Heath, G. A.; Newby, L.; Webster, R. D. *Chem. Commun.* **2002**, 754−755.
(27) Fortage, J.; Scarpaci, A.; Viau, L.; Pellegrin, Y.; Blart, E.; Falkenström, M.; Hammarström, L.; Asselberghs, I.; Kellens, R.; Libaers, W.; Clays, K.; Eng, M. P.; Odobel, F. *Chem.—Eur. J.* **2009**, *15*, 9058−9067.
(28) Fajer, J.; Borg, D. C.; Forman, A.; Dolphin, D.; Felton, R. H. *J. Am. Chem. Soc.* **1970**, *92*, 3451−3459.
(29) Szeghalmi, A. V.; Erdmann, M.; Engel, V.; Schmitt, M.; Amthor, S.; Kriegisch, V.; Nöll, G.; Stahl, R.; Lambert, C.; Leusser, D.; Stalke, D.; Zabel, M.; Popp, J. *J. Am. Chem. Soc.* **2004**, *126*, 7834−7845.
(30) In our preliminary communication,[5] we used 6-31G* as the basis set for H, C, N, P. For metals, LANL2DZ as basis sets and effective core potentials were used.
(31) The average Pd−C bond length calculated for **3c** (2.084 Å) is longer than that observed for **3b** [2.046(4) Å; X-ray]. This difference is attributable to the different coordination geometries at the zinc centers of **3c** (tetracoordinate) and **3b** (pentacoordinate). In **3b**, which was obtained by recrystallization from CH_2Cl_2−MeOH, the oxygen atom of the solvated MeOH coordinates to the zinc center as an axial ligand. Accordingly, the zinc atom is deviated by 0.32 Å from the mean porphyrin π-plane. See ref 5.
(32) The covalent-bond radii of 0.70 (for carbon), 1.37 (for palladium), and 1.38 Å (for platinum) are used.
(33) For reviews, see: (a) Stillman, M. J.; Nyokong, T. In *Phthalocyanines: Properties and Applications*; Leznoff, C. C.; Lever, A. B. P., Eds.; VCH: Weinheim, Germany, 1989; Vol. *1*, Chapter 3, pp 133−289. (b) Mack, J.; Stillman, M. J.; Kobayashi, N. *Coord. Chem. Rev.* **2007**, *251*, 429−453.
(34) (a) Michl, J. *J. Am. Chem. Soc.* **1978**, *100*, 6801−6811. (b) Michl, J. *J. Am. Chem. Soc.* **1978**, *100*, 6812−6818. (c) Keegan, J. D.;

Stolzenberg, A. M.; Lu, Y.-C.; Linder, R. E.; Barth, G.; Moscowitz, A.; Bunnenberg, E.; Djerassi, C. *J. Am. Chem. Soc.* **1982**, *104*, 4317−4329.
(35) (a) Kobayashi, N.; Miwa, H.; Isago, H.; Tomura, T. *Inorg. Chem.* **1999**, *38*, 479−485. (b) Kobayashi, N.; Lever, A. B. P. *J. Am. Chem. Soc.* **1987**, *109*, 7433−7441. (c) Kobayashi, N.; Ogata, H.; Nonaka, N.; Luk'yanets, E. A. *Chem.—Eur. J.* **2003**, *9*, 5123−5134.
(36) Guo, L.; Ellis, D. E.; Hoffman, B. M.; Ishikawa, Y. *Inorg. Chem.* **1996**, *35*, 5304−5312.
(37) Hartnell, R. D.; Arnold, D. P. *Eur. J. Inorg. Chem.* **2004**, 1262−1269.
(38) (a) Hurley, M. M.; Pacios, L. F.; Christiansen, P. A.; Ross, R. B.; Ermler, W. C. *J. Chem. Phys.* **1986**, *84*, 6840−6853. (b) LaJohn, L. A.; Christiansen, P. A.; Ross, R. B.; Atashroo, T.; Ermler, W. C. *J. Chem. Phys.* **1987**, *87*, 2812−2824. (c) Ross, R. B.; Powers, J. M.; Atashroo, T.; Ermler, W. C.; LaJohn, L. A.; Christiansen, P. A. *J. Chem. Phys.* **1990**, *93*, 6654−6670.
(39) (a) Dunning, T. H. Jr. *J. Chem. Phys.* **1989**, *90*, 1007−1023. (b) Woon, D. E.; Dunning, T. H. Jr. *J. Chem. Phys.* **1993**, *98*, 1358−1371.
(40) (a) Becke, A. D. *Phys Rev. A* **1988**, *38*, 3098−3100. (b) Becke, A. D. *J. Chem. Phys.* **1993**, *98*, 5648−5652. (c) Lee, C.; Yang, W.; Parr, R. G. *Phys. Rev. B* **1988**, *37*, 785−789.
(41) Cancès, M. T.; Mennucci, B.; Tomasi, J. *J. Chem. Phys.* **1997**, *107*, 3032−3041.
(42) Frisch, M. J.; et al. *Gaussian 03, Revision C.02*; Gaussian, Inc.: Wallingford CT, 2004.